Polynya Formation in Hudson Bay

During the Winter Period

by

Geoffrey Gunn

A Thesis submitted to the Faculty of Graduate Studies of

The University of Manitoba

in partial fulfilment of the requirements of the degree of

MASTER OF SCIENCE

Department of Environment and Geography

University of Manitoba

Winnipeg

ABSTRACT

Previous understanding of the winter ice regime in Hudson Bay was limited. This investigation demonstrates the existence of a large coastal polynya in northwestern Hudson Bay. Measuring approximately 600 km long by 60 km wide, this polynya is typically opened and maintained by surface winds for periods of one to five days. Closing mechanisms result from decline in wind maintenance and apparent thermodynamic ice formation. Open water is present on the northwest coast at some size for up to 70% of the winter between ice formation and breakup.

Observation of this open water during the period of the winter ice pack indicates that the 'ice factory', modelled previously, in northwest Hudson Bay exists. This furthers understanding of the freshwater budgets, stratification, and atmosphere-ocean interactions while presenting new questions about climate change and the future of the Hudson Bay physical system.

ACKNOWLEDGEMENTS

Thanks to the support, knowledge, and enthusiasm of my supervisor Dr. David Barber and committee members Dr. Jens Ehn, Mr. Pierre Larouche, and Dr. Greg McCullough. The thesis herein would not have been possible without the expertise and passion of the members of the Centre for Earth Observation Science at the University of Manitoba: the passion for Arctic science and discovery is infectious.

Financial support for this was provided by ArcticNET – a Network of Centres of Excellence; the Natural Science and Engineering Research Council (NSERC); the Northern Scientific Training Program; and Manitoba Hydro.

Special thanks to my family from whom I gained respect for science and nature. Especially thank you to my new wife Mallory, who has supported me the whole time (and told me to relax!).

DEDICATION

This thesis is built upon a foundation laid by the late Dr. Klaus Hochheim. the insight and mentorship he provided is hopefully apparent in this document.

Sumus nanos gigantum humeris insidentes

CONTENTS

LIST OF TABLES

LIST OF FIGURES

1 INTRODUCTION

The Arctic is changing. Concern is growing that the geophysical systems that underlie biological and human ecology are shifting to new equilibria. Summer sea ice has declined considerably, and winter climate systems have shifted (Stroeve et al., 2005; 2008; Overland et al., 2014). Understanding cryospheric interactions with the atmosphere, hydrosphere, and biosphere is essential in navigating a changing climate (Intergovernmental Panel on Climate Change [IPCC], 2013; Arctic Climate Impact Assessment [ACIA], 2005)

Hudson Bay is central to Canada's history and geography. History records the Bay as a meeting ground for the First Nations and Inuit; a gateway to European exploration following the ill-fated voyage of Henry Hudson; a battleground for fur and imperial influence over the continent; and most-recently a sea route for grain and minerals from the Canadian interior to the global economy. This northern sea has remained relatively understudied (Stewart and Barber 2010).

In an ocean-sea ice-atmosphere model presented by Saucier et al. (2004), a large sea ice anomaly was reported along the northwest coast of Hudson Bay. Later studies by Hochheim et al. (2011) provided the observational confirmation that a large anomaly existed during the spring ice breakup period. This thesis confirms the existence of a significant northwestern coastal polynya and describes likely forcing mechanisms using high resolution, frequent remotely-sensed data to determine daily changes to sea ice during the winter period in Hudson Bay.

1.1 Research Objectives

To support the hypothesis that there is a large, recurrent polynya in northwestern Hudson Bay this document investigates spatial, temporal, and forcing characteristics of sea ice in the area of interest. It examines the winter sea ice regime and associated atmospheric and oceanographic systems to answer the following questions:

1. Define morphology of the northwest polynya in Hudson Bay
2. Determine spatial and temporal variability of this polynya
3. Examine forcing mechanisms and atmospheric teleconnections to polynya formation.

1.2 Thesis Structure

This document is divided into five chapters plus an appendix. Chapter two discusses the literature behind this analysis: the first subsection is an overview of sea ice physical and geographical concepts from formation to motion – the influences and impacts of ice on the ocean; the next subsection examines the principles of sea ice remote sensing; finally a detailed review of the state of Hudson Bay physical research in relation to the ice and atmospheric climate.

Chapter three is a description of methods used in this investigation. The specific study area subregions are presented, followed by data sources used in the analysis. The analysis methods and framework are examined in the third subsection. Chapter four describes results from the analysis supporting objectives noted in §1.1, then discusses these findings including recommendations for future research. Chapter five is the conclusion followed by an appendix.

2 LITERATURE REVIEW

This literature review is intended to provide the philosophical and scientific context upon which this research is based. Section 2.1 discusses the physical basis behind sea ice formation and connections to oceanography. Section 2.2 examines the physical science of remote sensing and the research practices associated with the field; special focus is applied to techniques used in polar remote sensing of polynyas and leads. Section 2.3 reviews literature specific to the study area, Hudson Bay, and local research into the ocean-sea ice-atmosphere interface and biological connections.

2.1 SEA ICE AND OCEANS

Sea ice is an expression of the atmospheric and oceanographic climate at the interface of these systems. Extreme annual variance in solar radiation due to the Earth's tilt significantly affects the surface and atmospheric energy budgets, leading to parts of the year with a net positive energy budget (local summer) and parts of the year with a net negative energy budget (local winter). The balance of this energy budget, inferred with sea ice formation and melt dates, has been used to indicate climate change in the polar regions (Gagnon and Gough, 2005a; Hinzman et al., 2005; Markus et al., 2009). The following subsections describe the physical relationships between ice and oceans.

2.1.1 FORMATION

Sea ice is formed when cool air masses contact warmer surface waters and the resulting heat flux is great enough to reduce surface temperature below the freezing point of sea water, which is dependent on surface salinity. Air has a lower heat capacity than water (~1 J/g K vs. 4.18 J/g K) and thus is more susceptible to rapid cooling. Heat

flux is dominantly from water to air during autumn and winter. The reduction in density caused by loss of heat is often only enough to sink a parcel of water to the pycnocline – the first significant density gradient— which results in a vertically-mixing surface layer. This vertical mixing may also be supported by wind-generated turbulence as well. This means that only the volume of water above the pycnocline must be cooled to near-freezing until the process of fusion occurs (Petrich and Eicken, 2010). When the surface layer has reached the freezing point of the solution, small volumes of super-cooled water exist until they contact a nucleation particle to form a frazil ice crystal (Assur and Weeks, 1964).

Atmospheric factors direct the larger physical morphology of a new ice pack: the most significant is the kinetic energy of the sea water substrate on forming ice (Wadhams, 2000). There are two major paths of ice formation: the nilas-forming process and the pancake process. The nilas process occurs with low wave/wind energy conditions where once the upper water layer has cooled to its freezing point, crystals form on or near the surface. As frazil ice grows and collects at the surface, consolidating to form thin sheets of grease ice. These sheets in turn grow from the bottom, collecting buoyant frazil and granular ice crystals and nucleating ice on the bottom (Petrich and Eicken, 2010). Calm conditions allow these crystals to join together into a sheet of nilas ice. Nilas sheets are smooth and able to bend and flex with long period swells. Optically young nilas sheets have low albedo, preferentially transmitting light (Wadhams, 2000; Perovich, 2002). Spatial distribution of frazil ice can be affected by winds through Langmuir circulation: shallow vertical mixing of the water mass that moves the ice into

ordered bands parallel to wind forcing, separating newly-formed ice from open water (Pease, 1987).

Ice formation in rougher surface conditions causes the thin ice surface to break apart as wave-motion breaks the brittle axes of the ice crystal structure. Consistently rough water during formation prevents large sheets of nilas from remaining together and instead forms features called pancake ice (Tucker et al., 1992). Wave motion causes regular impaction of the ice pans, rounding edges and spraying them with near-freezing or super cooled water, growing margins preferentially with slush while continually forming frazil ice is broken into small crystals or joins the pans on the bottom (Petrich and Eicken, 2010). Pancakes can grow to 5 m in diameter when sheltered from intense wave action as they move deeper in to the marginal ice zone. As ice pans are compressed or driven into large pack ice wave motion dampens, nilas ice to form in the interstitial spaces cementing the pancakes into a sheet (Wadhams et al., 2000).

A contiguous sea ice sheet grows from the bottom. Congelation ice—nucleated on the bottom of the ice layer—becomes the largest constituent of a nilas-formed sheet or floe. Once the nilas has frozen over completely, heat flux between the water and air slows but does not stop completely. Ice will stop forming when equilibrium is reached between subsurface melt and fusion rates (Petrich and Eicken, 2010).

This process at the ocean-sea ice interface is important to the local freshwater budget. It causes small pockets of water to become trapped within the ice crystal framework. These pockets of sea water are frozen *in situ,* trapping salt ions and separating them from freezing water molecules. Salt ions trapped in these pockets

depress the freezing point of the remaining saltwater solution as the cell becomes smaller. Brine in the pockets is denser than the surrounding frozen water, causing slow gravity drainage as the liquid brine melts channels through the ice matrix towards the warmer surface water (Weeks and Ackley, 1986). Deformation caused either by differential thermal contraction of the ice matrix; or by physical dynamics, can expel large amounts of brine down to the water (Untersteiner, 1968; Cox and Weeks, 1975). Finally the brine channels may drain as ice formation on the bottom of the floe floats the top away from the surface, creating both the pressure and potential energy to force the dense brine through a system of channels and out of the floe.

This overall process of brine rejection is a significant contribution to the thermohaline circulation in polar seas (Aagaard and Woodgate, 2001). Stratification is reduced in Arctic seas over sites of significant ice production; motion of dense water masses due to gravity mixes upper water masses along coastal shelf margins to form the upper halocline layer (Aagaard et al., 1981; Melling and Lewis, 1982). Stronger summer stratification can be forced by a thicker, fresher ice coverage or terrestrial freshwater inputs. Strength of stratification in turn affects primary production, nutrient cycling, and further seasonal sea ice formation (Sverdrup 1953; Aagaard and Carmack, 1989; Aagaard and Woodgate, 2001; Behrenfeld, 2010; Ferland et al., 2011).

2.1.2 MOTION

Ice motion is forced by the atmosphere and ocean. Whether a given ice floe is moved or deformed by these forcing mechanisms is a factor of ice rheology and strength – which are in turn determined by the thermodynamic development, growth

stage, and thickness of the floe. Factors influencing motion of ice include air stress, water stress, Coriolis force, internal ice stress, and force due to sea surface tilt (Wadhams, 2000). In most conditions air stress and water stress are the dominant factors in the motion of sea ice, with the Coriolis force (the approximation to account for apparent deflection of fluids on a rotating solid Earth) accounting for alterations to the movement vector (Thorndike and Colony, 1982; Wadhams, 2000). The motion vectors of an ice pack are typically 2% of the surface wind speed with a heading +30º of the wind direction (Thorndike and Colony, 1982).

Ice floes converge when movement of waves puts opposing floes out of phase or wind drives them together, potentially against a larger, less mobile body such as a coastline, grounded iceberg, or fast ice. When two ice floes contact each other, one of two processes occur: rafting or ridging. Rafting involves one sheet being forced over another creating a large interface for the pieces to freeze together and form thick consolidated areas. Rafting can also be more complex, wherein the pieces interlock (Thorndike et al., 1975; Babko et al., 2002). This process is relatively infrequent, as it requires relatively thin ice sheets contacting in specific conditions.

The more common convergent process is ridging. This process takes place when two floes—or a single floe with a weak joint or linear feature such as a refrozen lead—are compressed with the broadsides meeting. The edges are forced away from the axis of convergence to form identifiable 'sails' above the ice and 'keels' below (Wadhams, 2000). This energetic impact may consolidate the affected ice sheets with strong joints that can endure for the lifespan of the ice sheet. Pressure ridging is visible on most ice

floes and can be a major source of surface roughness on either side of ice sheets, increasing overall ice thickness and allowing for increased ice production (Wadhams, 2000). These features in turn increase susceptibility to forcing by increasing atmospheric and oceanic friction.

2.1.3 DECAY

Melting is a seasonal process in the Arctic Ocean that occurs when the overall energy balance at the surface is positive. Sea ice decays as the energy flux changes from ocean-to-atmosphere to atmosphere-to-ocean. Higher spring and summer sun angles increases incident solar radiation, although warm southern airmasses, advection to lower latitudes, and warm water currents may also affect the energy balance. Despite the high initial albedo of thick sea ice and snow, the nonzero absorption of solar energy slowly begins the gradual melt process until ponds form on the surfaces of ice sheets. These melt ponds lower overall albedo and enhance absorption of visible light (Perovich, 2005). This further warms the ponds that, depending on local topography, can deepen and melt into the ice.

The melt location of mobile ice has an impact on local oceanography and cascading effects to the biosphere. After brine rejection, first year sea ice has a lower salinity than the sea water it floats upon (Wadhams, 2000). Like distillation writ large, this fresh water is returned to the surface layer during the melt stage of the ice life cycle. Lower density meltwater floats on the surface or freshens the upper mixed layer (Aagaard and Woodgate, 2001). Holland et al. (1996) determined this process contributes significant maintenance the mixed layer in the Arctic Ocean. This can be contrasted to the

distillation enabled by evaporation at equatorial and temperate latitudes, which is relatively weak in polar areas.

2.1.4 FAST ICE

Mobile sea ice discussed thus far is differentiated from sea ice that is in some way fixed to a surface, called fast ice. This ice is essentially motionless, as the dynamic inputs it experiences are insufficient to overcome the friction or strength of the media in contact with the ice. Typical shore fast ice is often attached to a beach or coastline by a "foot" – ice that directly contacts the beach stretching from the high tide to low tide points (Wadhams, 2000). Beaches and shallow coastline gradients are the most common environments for landfast ice to form; rocky headlands or areas with significant current and wind forcing are less likely to form this ice feature (Wadhams, 2000).

The shallow coastal areas form ice faster, as a lower volume of water needs to be cooled to the freezing point. The freezing point may be higher due to a freshwater layer from overland runoff inshore (Granskog et al., 2009). Lower local salinity preceding summer melt distributions, and surface air temperature can impact spatial distributions of formation and thickness (Gough et al., 2004a).

2.1.5 POLYNYAS AND LEADS

Polynyas are geographical features that are unique from their surroundings: they are recurring or persistent areas of lower sea ice thickness, concentration, or extent (Barber and Massom, 2007). Named by Russian whalers – to whom these featured appeared to be lakes among an expanse of solid ice – they have been known to harbour

unique physical and biological diversity (Stirling, 1980; Dunbar, 1981; Massom et al., 1998; Lemke, 2001; Arrigo and van Dijken, 2003). Although the name 'polynya' dates to at least the 19th century, there is evidence that circumpolar peoples have used polynyas for subsistence or economic purposes for at least 3000 years (Schlederman, 1980).

Polynya type nomenclature varies throughout the literature and rarely has a single, overall definition been widely accepted. The most common bifurcation of polynyas is by forcing mechanisms, clarified by Smith et al. (1990). Sensible heat polynyas (also known as thermodynamically-forced polynyas) are caused by heat flux from relatively warm, dense waters forced upwards by bathymetric features or ocean currents. Latent heat (or dynamically/mechanically-forced) polynyas are caused by persistent or intermittent wind moving ice away from a shore or otherwise land-fast surface (Pease, 1987, Smith et al., 1990, Morales Maqueda et al., 2004). In these polynyas both the advection of solid ice and latent heat released from freezing ice maintains the polynya opening (Pease 1987, van Woert 1999). Most polynyas exhibit characteristics of each type: it is generally presumed that the strongest, most persistent polynyas are influenced by both oceanic and atmospheric factors to some extent (Morales Maqueda et al., 2004). The commonality between both types is thin or no ice when atmospheric conditions alone would suggest larger-than-observed ice thickness.

Leads are also features typified by an irregular absence of sea ice. Leads are linear cracks in ice that are formed by divergence forced by sea currents or surface winds. Leads may regularly concentrate in certain areas, but size and orientation is entirely variable (Williams et al., 2007). Latent heat polynyas and leads are similar in that they

share a forcing mechanism (Smith et al., 1990); however the morphology of this expression – relating to both the ice strength and recurrence of forcing mechanism – determine whether a polynya or a lead is formed.

Ocean water exposed in a polynya or lead is considerably warmer than the atmosphere. Without the insulation of sea ice these areas result in considerable heat flux, orders of magnitude greater than the surrounding ice-covered surface (Maykut, 1978, 1982; Dieckmann and Hellmer, 2009). This flux has two major results: increased ice formation as heat moves from the ocean to the atmosphere (Cavalieri and Martin, 1985); and the upwelling oceanic heat modifying local atmospheric conditions (Pinto et al., 1995; Pinto, 2003). Later in the season there may be a net gain of energy input to the water. Increased solar radiation can heat the open water – due to considerably higher absorption of dark, absorptive water relative to reflective snow and ice – and precipitate rapid localized melt (Hall and Rothrock, 1987; Massom et al., 1998).

Causes of the most studied latent heat polynyas are katabatic winds moving downslope on Antarctica (Bromwich and Kurtz, 1984; Pease, 1987; Reddy et al., 2007; Kern, 2008), and geostrophic or otherwise persistent winds in the Arctic (McNutt, 1981; Stringer and Groves, 1991; Cavalieri and Martin, 1994; Fu et al., 2012). At both poles these dynamically-forced polynyas have been implicated in the production of dense water and formation of summer surface-layer stratification (Morales Maqueda et al., 2004). Pease (1987) produced a one-dimensional model accounting for forcing influences on the growth, maintenance, and decline of a latent heat polynya. The author determined that wind velocity only partially accounts for latent heat polynya

maintenance: air temperature affects ice growth rate and can easily upset the balance to a negative growth rate. A key finding from this model was that for wind speeds of greater than 10 m s^{-1} the increased momentum transfer is offset by increased heat flux, which in turn produces ice more rapidly than it can be advected.

Coastal polynyas are commonly referred to as ice factories due to disproportionate production of young ice (Lemke, 2001; Kern et al., 2007; Williams et al., 2007; IPCC, 2013). During polynya activity, ice morphology in these areas follows a gradient of thickness from open water through unconsolidated frazil ice to a thermodynamically driven thickness proportionate to the surrounding icepack. If the mechanical maintenance mechanisms decline, stop, or reverse the equilibrium shifts to ice congelation. This continues with a below-freezing surface air temperature, replacing the polynya with a region of thin—yet still consolidated—ice pack. This ice is mechanically weaker than the surroundings, and a reversal of forcing mechanisms may produce a more disproportionately ridged or rafted pack than the surroundings (Prinsenberg, 1988).

Alongside this ice production is brine rejection (§2.1.1). Ice production in polynya regions may occur multiple times per winter season, leading to significant fluxes of brine from surface waters to shelf or deep water (Aagaard et al., 1981; Martin and Cavalieri, 1989). Given enough momentum, brine rejection (from rapid ice formation) causes penetrative convection, eroding the stable, dense layer and growing the active mixed layer (Kato and Phillips, 1969; Moroni and Cenedese, 2006). Few polynyas are studied

during the active period to quantify salt and freshwater flux in the watermasses below (Kirillov et al., 2013).

Measurement of polynya geometry depends on fluid geographical definitions of limits, boundaries, and processes. Williams et al. (2007) splits the geometry of a polynya into two metric categories and two operational categories: an open water region and a mixed ice-water region; or a practical polynya – where travel is unsafe – and a full polynya which encompasses the complete area of no- or thinner ice than the wider region. Liu et al. (1997), Morales Maqueda et al. (2004), and other remote sensing/modelling studies focus on the first two which act respectively as the open water/frazil production zone and the floe agglomeration zone. The measurement of the open water zone has more utility for heat flux estimates, while measurement of the entire disturbed area is important for sea ice growth rates, oceanographic influences, and biological habitat studies (Stirling 1980; Massom 1988).

2.2 Remote Sensing of Sea Ice

Satellite remote sensing allows researchers and interested professionals to understand processes, systems, and events at or above the Earth's surface on significant spatial and temporal scales. Earth Observation (EO) has significantly altered the academic pursuit of physical geography and increased the products available for commercial, governmental, transportation, and geophysical research by providing frequent high resolution imagery with a variety of wavelengths and illumination sources.

There are two principal modes of remote sensing: measurement of emitted radiation, and measurement of reflected radiation. Measurement of emitted radiation

relies on the property of all matter above 0 Kelvin (approximately -273°C) to radiate energy in accordance with properties which are determined by the temperature and emissivity of the specific type of matter. Measurement of reflected relies on some other source of incident energy – commonly the sun or the instrument itself – reaching the target with a fraction of this returned to the sensor. The former method is typically used in the passive microwave (PMW) and thermal infrared (TIR) methods, while the latter is used in optical/visible light and active microwave methods.

Sea ice has unique interactions with thermodynamic and electromagnetic radiation, allowing research to be performed on spatial variability and temporal change of geophysical properties (Winebrenner et al., 1992; Barber, 2005). From a materials science perspective, it may be thought of as a complex alloy of water, air, and solid and/or dissolved salts (Sihvola and Kong, 1988, Barber, 2005). Interactions of these materials with energy has been modelled extensively (e.g. Swift et al., 1985; Hwang, 2007; Spreen et al., 2008). From these models there have been attempts to derive important geophysical parameters of sea ice, such as thickness, extent, age, and surface roughness.

This section will examine principals and history of remote sensing of sea ice with passive microwave radiometry and the spatial, temporal, and anomaly detection methods relevant to this investigation.

2.2.1 Passive Microwave Radiometry and Sea Ice

The Passive Microwave (PMW) spectrum has been used to measure sea ice since the first sensor, the Electronic Scanning Microwave Radiometer (ESMR), was launched

aboard the Nimbus-5 satellite in 1972. Utilizing atmospheric windows in the microwave portion of the electromagnetic spectrum, many atmospheric phenomena like clouds are less opaque and may be calibrated for. In addition to the ability to make detections without incident sunlight (as opposed to optical sensors), these characteristics made PMW a highly desirable choice for long-term analyses of sea ice concentration.

Passive microwave datasets report calibrated brightness temperatures (T_B): the modelled temperature at which theoretical blackbody produces sensor-incident microwave radiation at the collected frequency/wavelength. Diversity of matter upon the Earth's surface generally precludes actual temperature calculation without surface truthing calibration, but this relationship between brightness temperature and type matter is utilized in remote sensing to determine type and distribution of surface cover. Early studies attempting to relate sea ice geophysical variables like concentration used simple unmixing algorithms to derive products from sensor brightness temperatures (Comiso and Zwally, 1989).

Later sensors added more frequencies and polarization orientations to improve spatial resolution (~89 GHz) and reduce atmospheric interference (~37 GHz). Two algorithms dominate ice concentration research: the NASA Team and the Bootstrap (Cavalieri et al., 1990; 1999; Comiso and Kwok, 1996). The NASA Team algorithm is a semi-analytical approach using the polarization ratio and gradient ratio between 19V, 19H, and 37V GHz polarization channels. The Bootstrap algorithm uses known concentration tiepoints in the high ice concentration and low concentration regions of the poles, integrating concentration between them. Both algorithms have been used

for hemisphere-scale measurements of ice concentration and extent (Parkinson et al., 1999; Parkinson, 2000). The number of existing algorithms requires careful consideration of the appropriateness for the target and location of interest: there are many factors that can confound algorithm calibrations. Sources of error include thin ice, snow melt, and unexpected atmospheric effects (Grenfell et al., 1992; Cavalieri et al., 1995; Comiso and Kwok, 1996; Fetterer and Untersteiner, 1998).

Kaleschke et al. (2001) began development of the ARTIST Sea Ice (ASI) algorithm to take full advantage of high resolution 85 to 89 GHz frequencies available on a newer generation of orbital passive microwave radiometers. Based upon a polarization differencing technique, this algorithm been used in the measurement of coastal or otherwise constrained environments (Kern 2008; Spreen et al., 2008; Smith et al., 2011; Rohrs and Kaleschke 2012; Cape et al., 2014; Jardon et al., 2014). This high resolution limits mixed pixels discarded due to terrestrial contamination. In a comparison to active microwave techniques, Heinrichs et al. (2006) determined that the ASI algorithm was comparable for presence/absence of ice extent in coastal and marginal ice areas.

2.2.2 Spatial Measurement of Sea Ice

Satellite measurement of sea ice and related phenomena is associated with the inherent limitations to orbital remote sensing. A sensor field of view imparts a spatial resolution; sensor calibration and design can determine a radiometric resolution. Orbital characteristics and sensor field of view impart a temporal, or recurrence, resolution. However the remoteness of the target and necessity of investigation makes remote sensing an appropriate supplement to *in situ* and modelling investigations.

Orbital remote sensing of sea ice is typically concerned with mapping spatial distributions of ice and measuring ice age, and thickness while minimizing limitations inherent to this mode of analysis (Lubin and Massom, 2004; Comiso, 2010).

The simplest spatial measurement of sea ice is sea ice concentration (SIC) – that is the percentage of a given area covered by solid ice relative to the given area (Lubin and Massom, 2004). This may be communicated for a whole region (i.e. physical feature or region of interest) or for a minimum mapping unit (i.e. a single polygon or pixel).

Sea Ice Extent (SIE) is a measurement intended to calculate the total area of sea ice above a defined concentration threshold. The National Snow and Ice Data Center (NSIDC), a division of the United Stations National Oceanographic and Atmospheric Administration (NOAA), defines ice extent as the sum of all mapping units above a 15% SIC threshold for sea ice concentration products. Typically an extent threshold is determined based on the spatial property of interest, as a method to minimize error in sea ice concentration values, and to measure different ice types that correlate with concentration (Table 2-1).

Table 2-1 - Use of Sea Ice Thresholds in Literature

Article	Target	SIC Threshold(s)
Smith et al. 2011	Dumont d'Urville Sea; Mertz Glacier Polynya	<10%, 11-79%, >80%
Arrigo et al. 2003	37 Arctic Coastal Polynyas	>10%
Massom et al. 1998	Antarctic latent-heat polynyas	≥75%
Worby et al. 2004	Antarctic ice edge/marginal ice zone	>15%
Heinrichs et al. 2006	Bering Sea ice edge/marginal ice zones	>15%

Sea Ice Area (SIA) is the calculated area of a region covered by sea ice less the area covered by open water. Using raster-type (gridded) data, this is calculated as:

Equation 1 - Sea Ice Area

$$-A_i = \sum (C_t * A_{cell})$$

where A_i is the SIA for a given region, C_t is the SIC for a given cell (expressed as a percent), and A_{cell} is the area for the given subregion, or the spatial resolution squared. For a complete area this is summed from all constituent subregions – typically raster cells or polygons.

Sea Ice Volume (SIV) represents a three-dimensional property of the given area of ice. This can only be calculated if there are thickness estimates or measurements from a sea ice feature: often absent from remote sensing data products. In an analysis of Foxe Basin, Ersahin et al. (2011) utilized Canadian Ice Service Operational Ice Charts to calculate pseudo-ice thickness as a gridded raster variable using the following formula:

Equation 2 - Polygon Ice Thickness (Ersahin et al., 2011)

$$S_t = \sum^{n} (C_a * S_a) + (C_b * S_b) + \ldots + (C_n * S_n)$$

Where S_t represents the total grid cell thickness, C_n represents the percent concentration of the given area, and S_n represents the stage of development/estimated thickness (Canadian Ice Service [CIS] 2006). Essentially this is a weighted mean of thicknesses that correspond to the EGG code methods of ice observation provided as operational ice products by CIS.

2.2.3 POLYNYA DETECTION

The strict definition of a polynya includes both open water area and areas of reduced or thinner ice coverage (§2.1.5). Methods for measurement of polynya area and variability may be defined differently depending on the underlying research theme. A polynya to a researcher measuring carbon fluxes may be different to a researcher measuring marine mammal habitat. This section reviews literature focused on detection, measurement, and analysis of polynya-susceptible regions.

Early techniques for polynya detection involved thermal infrared (TIR) and Landsat Multi-Spectral Scanner (MSS) optical datasets due to significant differences in emission between warm open water and cold sea ice or white ice and dark water pixels, respectively (Dey et al., 1979; Smith and Rigby 1981). Spatial resolution of these datasets were nearly two orders of magnitude higher than available passive microwave at the time, and for single event or single season analyses these methods had proven utility (Stringer and Groves, 1991). As noted above, darkness, cloudcover, and infrequent return periods for Landsat and AVHRR precluded a comprehensive census of

polynya activity over a given period. These studies could determine polynya presence in an area with optical confirmation of an in-progress polynya event or thin ice indicative of a recently open polynya.

Markus and Burns (1995) developed the Polynya Signature Simulation Method (PSSM) to increase utility of relatively low resolution SSM/I passive microwave data to map small Antarctic polynyas, many of which are less than one SSM/I pixel. This method used the relationship between collected brightness temperatures at 85- and 37-GHz to leverage the higher spatial resolution of the former frequency and the minimal atmospheric effects of the latter. This method simulates brightness temperatures for sea ice classes (sea ice, shelf ice, open water) – based on areas of known surface coverage – coevolved with potential antenna patterns to find the best agreement between simulated class and actual pixels. This method was developed to investigate the for Antarctic polynya system (Arrigo et al., 2003; Kern 2009; Arrigo et al., 2012) but has been used in marginal seas of the Arctic Ocean as well (Willmes et al., 2011). A significant limitation to this method is the requirement of proximity to known validation points for ice. It is relatively easy around the Antarctic continent to be proximal to shelf ice, sea ice, and open water, but this method is met with difficulty in the land-bordered Arctic Ocean (Willmes et al., 2011).

The principal reason for using PSSM and other sub-pixel unmixing methods was the amount of error coastlines and mixed pixels can impart on important near-shore open water investigations through heavily mixed pixels between ice, open water, fast

ice, and terrestrial ice. With the advent of higher-resolution passive microwave, research on coastal polynyas returned to using sea ice concentration and sea ice extent.

Sea ice extent (SIE) has been used for polynya studies throughout the passive microwave era. It has demonstrated utility for measurement of ice edge locations in Antarctica (Jacobs and Comiso, 1993), and for polynya detection studies (Bareiss and Görgen, 2005). Passive microwave algorithms impart error in their estimation of sea ice concentration, and the use of a conservative threshold reduces sources of error caused by thin, complete ice or surface melt ponds (Heinrichs et al., 2006). As noted above, Heinrichs et al. (2006) determined that a 15% SIC threshold is optimal for near-coastline and polynya use with passive microwave radiometry. Radiometric thresholding such as SIE has a long history in the practice of remote sensing outside of sea ice research (Lillesand et al., 2008). Classes applied to single or multiple bands reduce dimensionality for spatial and temporal analysis. Thresholds have utility in polynya analyses to reduce atmospheric effects of water vapour and fog that may cause PMW algorithms to over- or underreport ice concentration and open water. Recently, this technique has been used to measure ice movement and polynya processes in concert with various PMW SIC algorithms, including the ARTIST Sea Ice algorithm (e.g. Fu et al., 2012; Smith et al., 2011). For spatial-temporal analysis of known or suspected polynyas, Bareiss and Görgen (2005) introduced an *a priori* mask based on examination of ice climatology, forcing mechanisms, and visual examination of the affected area. This method assisted not only with calculations of polynya area, but also with frequency and occurrence mapping(Kirillov et al., 2013).

2.3 HUDSON BAY MARINE COMPLEX

The Hudson Bay Marine Complex is a system of water bodies connected to the Arctic Ocean via the northwest passages through the Canadian Archipelago. The system represents one of the most unique large marine areas in the world – supporting an Arctic ecosystem complete with seasonal ice coverage extending to southern latitudes. The continental situation of the bay, and resulting large inputs of freshwater, and polar climate make Hudson Bay a natural laboratory for understanding processes relevant to the greater Arctic Ocean.

Hudson Bay is the world's largest inland sea (Prinsenberg, 1984; Martini, 1986) with a total marine area of 1.24 million km^2 (Saucier et al., 2004). The bay is a saline subarctic marine system that experiences a full cryospheric cycle each year – experiencing at times complete ice coverage (typically between January and April) and complete open water coverage (typically between late July and November). The complex is unique as a body of water due to the high inputs of Arctic water masses, large amount of surface runoff, complex coastal morphology, and nearly-complete annual ice coverage (Stewart and Barber, 2010).

2.3.1 PHYSICAL OCEANOGRAPHY

Arctic water enters Hudson Bay from Foxe Basin via Roes Welcome Sound, a shallow passage in the northwest between the North American mainland and Southampton Island. Beyond Hudson Strait and Foxe Basin, however, there is small enough exchange of water that researchers have declared the Hudson Bay Marine Complex as a relatively closed system in regards to ocean currents and water mass

exchange (Wang et al., 1994). Stratification is highly determined by the winter sea ice coverage through brine rejection (discussed above) melt of the ice pack, and fresh river water (Prinsenberg 1988, Prinsenberg 1986a). Brine rejection from ice formation deepens the Polar Mixed Layer (PML), a less dense water mass above the cold saline bottom water.

Currents in the bay are cyclonic, driven primarily by atmospheric momentum imparted on the sea surface (Prinsenberg, 1986a, Saucier et al., 2004). Vorticity is strengthened by summer atmospheric forcing, reaching a maximum at the end of the open water period. During ice coverage this circulation slows to a minimum at the end of the ice covered period (Prinsenberg, 1983; Prinsenberg, 1986a). This circulation creates a coastal freshwater conduit of more buoyant river input water that resists mixing into the upper mixed layers (Granskog et al., 2011).

Runoff water, precipitation, and sea ice melt are major contributing factors to the freshwater budget of Hudson Bay with runoff water and sea ice contributing a significant amount of variability (Prinsenberg, 1984; Jones and Anderson, 1994; Straneo and Saucier, 2008). Surface runoff contribution is approximately 0.9 m averaged over the bay's area, or 760 km^3, which totals 12% of the total pan-Arctic runoff (Déry et al., 2011, Lammers et al., 2001). Additional freshwater inputs from ice melt and runoff bring total freshwater inputs to 2.2 m distributed across the bay (Prinsenberg et al., 1987). Hudson Bay receives freshwater runoff a considerable watershed (Shiklomanov et al., 2000). This water mass stratification has been shown to be a major factor in the local climate, sea ice production, nutrient transport, and biological productivity

(Drinkwater and Jones, 1987; Markham, 1986; Prinsenberg, 1988; Hochheim et al., 2010).

Freshwater inputs are chemically different from oceanic inputs, and have been studied independently using tracers (Déry et al., 2005; St-Laurent et al., 2011). Depth of runoff-derived surface layer is inversely related to the sea ice melt water, indicating a displacement of one freshwater source for another. Seasonally, the upper stratification of Hudson Bay appears dependent on volume and distribution of ice melt, proximity to the coast, and amount of brine-rejection-induced gravity mixing during the previous winter.

The Hudson Bay marine system experiences a semi-diurnal tidal cycle with the principal lunar semi-diurnal constituent reaching 1.25 m on the west coast and up to 4 m in Churchill during the ice free season (Prinsenberg and Freeman, 1986). Two co-tidal points were determined in a model by Freeman and Murty (1976) as one northwest of the basin centre; and one due north of the Belcher Islands. Seasonal ice coverage tends to constrain tides, advancing arrival while reducing magnitude (Prinsenberg and Freeman, 1986). Results from a model by Kowalik and Proshutinsky (1994) demonstrated that tidal fracturing of the first year sea ice may be a contributing factor to ice production and deformation, with a maximum effect in the northwestern offshore quadrant of Hudson Bay.

2.3.2 Sea Ice Regime

Prior to the 1940s the dominant view was that Hudson Bay was mostly ice free during the winter months, with the exception of large fast ice shelves and some drifting

floes (USHO, 1946; Hare and Montgomery, 1949). However with increased air traffic during the Second World War pilots reported a significantly ice covered area, with few areas of open water during the winter months (Danielson, 1971). During the middle of the 20th century occasional overflights were made of the bay to report on sea ice conditions, culminating in Danielson (1971) reporting a nearly 100% ice cover during winter (January – April) with the exception of small leads along the east and west coast, 5 miles from a fast ice shelf on the west coast and 2 miles from the fast ice in the east. The author also reported frequent narrow leads surrounding Southampton Island.

Historical and recent spatial representations of sea ice formation and melt can be found in Danielson (1971), Markham (1986), Etkin (1991), Stirling et al. (1999), Gough et al. (2004), Gagnon and Gough (2005b), Joly et al. (2010), Hochheim et al. (2010), Hochheim and Barber (2010), Scott and Marshall (2010), and Hochheim et al. (2011); amongst others. The literature describes formation as beginning in shallow, coastal areas of Hudson Bay to the south and west. The deeper central and eastern sections freeze later. As discussed above, this early formation may arise from the congelation of fresher waters in the coastal conduit system and preconditioning of temperature in surface waters from the previous season's atmospheric and oceanic systems (Galbraith and Larouche, 2011; Gagnon and Gough, 2004; Hochheim and Barber, 2010). There is support for a bi-modal formation and melt regime along the east-west axis of the bay rather than a single consistent pattern for ice melt and formation (Hochheim et al., 2011; K. Hochheim pers. comm., 2013).

Knowledge of sea ice thickness in the bay remains based on estimates (Prinsenberg, 1988). Thicknesses typically reported from 1 m in James Bay near Moosonee to 2 m in Foxe Basin with variable maximum thicknesses in intermediate latitudes (Prinsenberg, 1988). *In situ* measurement has been performed on fast ice thickness and relationships to atmospheric forcing mechanisms (Gough et al., 2004a); however a high-resolution analysis of winter ice thickness distribution is lacking.

Wang et al. (1994) indicate that there may have been a change to the winter sea ice regime during a "climatic jump" in the early 1960s, in part signalled by a polynya appearing south of Southampton Island during the winters of 1961-1964. This polynya (Wang et al., 1994: Figure 10) is reported to be open during winter and spring and located in the central part of the basin to the south of Coats Island. Scott and Marshall (2010) reported a similar jump in the sea ice regime – signalled by a 12-day earlier mean breakup date – during the 1988-1989 winter season. Recent studies indicate a trend of earlier breakup still, as much as 3.2 days per decade (Gagnon and Gough, 2005a; Hochheim et al., 2011).

These sudden alterations to the sea ice have significant impacts on the icescape: the medium upon which considerable ecological diversity is dependent. Important species populations such as the Western Hudson Bay polar bear population (Stirling, 1977; Stirling and Ramsay, 1986; Stirling et al., 1999; Lunn et al., 1997) ringed seals (Chambellant et al., 2012), and beluga whales (Stirling, 1980; Stewart and Lockhart, 2005; Bhiry et al., 2011) are affected by changes in the character and duration of seasonal ice.

2.3.3 Atmospheric Influences

The literature demonstrates Hudson Bay is mainly controlled by large-scale atmospheric systems (Wang et al., 1994; Mysak et al. 1996; Tivy et al. 2011; Qian et al. 2008; Joly et al., 2010). Distance from the warming and moderating influence of oceans allows Hudson Bay to experience a uniquely continental climate for a such large body of water (Maxwell, 1986). In hemispheric-level studies of sea ice, there has been suggestion that anomalously high years of Hudson Bay ice cover was related to negative Southern Oscillation (SO) index values (Parkinson et al., 1999) while direct investigations of the bay revealed associations between positive SIE anomalies and the low/wet phase of the SO; and to the strong westerly phase of the North Atlantic Oscillation (NAO) (Wang et al., 1994). Mysak et al. (1996) examined years with both of these oscillations in phase finding significant positive anomalies in SIE, particularly in an increased consolidated ice period through a later breakup period. These positive extent anomalies were in some cases correlated with low surface air temperature during the melt/breakup period. Etkin (1991) performed a sensitivity analysis which demonstrated that an overall climate warming of 1°C would advance spring breakup by over two weeks in eastern parts of the bay.

The bay is situated at the margin between the cold polar high pressure Hadley Cell and the midlatitude westerlies. The Arctic front, as this boundary is known, is the trough between cold Arctic air and intermediate polar air masses across midlatitude North America, with the Polar front as the southern margin of this cold air extent (Oliver and Fairbridge, 1987). This Arctic front is the site of regular polar lows with frequent recurrence of a low-pressure system centred upon the south side of Baffin Island (Reed

1960; Maxwell 1986; Gyakum et al., 1996). A northern hemisphere mesoscale cyclone such as the Baffin Island low will rotate cyclonically, moving winds to the south in a positive zonal (west to east) direction. At a given point south of the Arctic front the geostrophic wind tendency will favour these persistent west winds. If the front pushes south winds will tend to shift to a negative zonal (east to west) vector, reversing direction. These shifts have been demonstrated to happen very quickly (Stewart and Barber, 2010). Proximity to a recurrent low pressure system through both wind vectors and surface air temperature has been shown to impact the sea ice system of Hudson Bay (Larouche and Dubois, 1988; Saucier et al., 2004; Hochheim and Barber, 2010; Hochheim et al., 2010, 2011; McGovern 2013).

2.3.4 Northwestern Hudson Bay Polynya

Previous studies have examined the spring sea ice regime of Hudson Bay (Hochheim et al., 2011; Scott and Marshall, 2010; Gough et al., 2004b; Gagnon and Gough, 2005b; McGovern, 2013), however the northwest coast has only been studied at a lower resolution (e.g. Wang et al., 1994); in addition to a greater area (e.g. Scott and Marshall, 2010); or as only a small portion of a greater climatological analysis (e.g. Saucier et al., 2004; Hochheim et al., 2011). A changing global climate in general, and polar regions in particular (IPCC, 2013), may lead to significant changes in sea ice regimes. Hudson Bay's climate is predicted to warm using General Circulation Models (GCMs), and sea ice is modelled to be a significantly altered feature in these scenarios (Gough and Wolfe, 2001; Gagnon and Gough, 2005a). The northwestern coast in particular and the coastline and islands of Hudson Bay in general may be significantly

affected by changing characteristics in ice coverage which has cascading effects to both the ecosystem (Stirling, 1980) and economy (Tivy et al., 2007; Stewart et al., 2012).

The northwest coast is an area of significant ecological importance (Stirling et al., 1977; Stirling, 1980; Lunn et al., 1997; Stirling, 1997; Dyck et al., 2007; Kuzyk et al., 2009; Chambellant et al., 2012; Regehr et al., 2007). There is a particularly strong relationship between the western Hudson Bay polar bear population and dates of breakup and formation (Regehr et al., 2007), although a study on this polynya in particular has not yet been performed in detail despite proximity to the Western Hudson Bay polar bear population (Lunn et al., 1997).

Maps of Arctic polynya distributions demonstrate that there is a shore lead complex in Hudson Bay, occasionally noting a polynya within Roes Welcome Sound (Danielson, 1971; Smith and Rigby, 1981; Stirling et al., 1981; Markham, 1986). Cartographic representation of the winter Hudson Bay ice regime indicates a small flaw lead ("approximately 5 miles wide" according to Danielson, 1971) between the shore fast ice and the central ice pack. In 2004 Saucier et al. published results from a regional sea ice-ocean model applied to the Hudson Bay Marine Complex. This demonstrated a large area on the northwest coast from Roes' Welcome Sound to Cape Churchill revealing a significant anomaly in salinity flux, ice production, and low mean sea ice concentration during winter months (Saucier et al., 2004 Figure 12(a)). The authors noted a large, well-defined feature with the hypothesis that it was dynamically forced by surface winds, a statement supported in principle by findings from Prinsenberg (1988); Gough and Allakverdova (1999); and Gough et al. (2004a). These studies support the

atmospheric forcing hypothesis as there appears to be insufficient heat flux moving through the inlet at Roes' Welcome Sound to account for the sea ice anomaly. There has been little observational research on this feature since.

If a large dynamically-forced polynya did exist along the northwest coast, modelled results from Saucier et al. (2004) demonstrate that overall ice thickness in that region would be lower, with less density stratification than other parts of the bay due to focused brine rejection and increased wind-mixing. Observations of the ice area would indicate intermittent periods of open or nearly-open water, frazil ice distributed in rows perpendicular to the shore, growing as heat moves out of the water area, and an increasingly consolidated icepack offshore. A fraction of that ice production would be caused by a tidal node in the northwest quadrant of the bay (Prinsenberg and Freeman, 1986; Kowalik and Proshutinsky, 1994). A significant amount of ice production would be unaccounted for without the existence of this polynya (Prinsenberg, 1988; Saucier, 2004).

3 METHODS

3.1 STUDY AREA

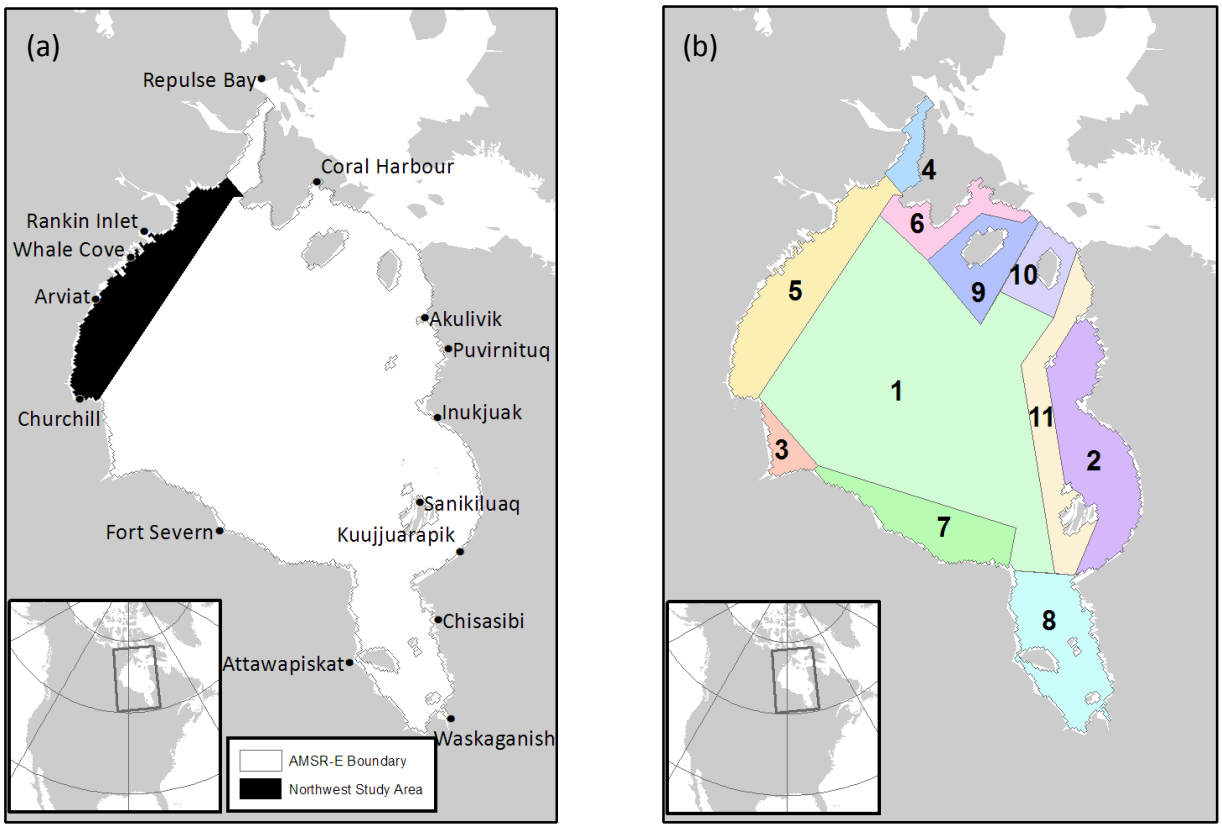

Figure 3-1 –(a) Northwest Hudson Bay Area of Interest; (b) Subregions (refer to Table 2-1)

Limits to the study area were defined to coincide with the International Hydrographic Organization *Limits of Oceans and Seas* (1953), which define Hudson Bay as:

On the North:

> A line from Nuvik Point (62º21' N, 78º06'W) to Leyson Point, a Southeastern extreme of Southampton Island, through the Southern and Western shores of Southampton Island to its Northern Extremity, thence a line to Beach Point (66º03' N, 86º06'W).

This analysis separates Hudson Bay proper from the rest of the Hudson Bay Marine Complex (HBMC) (Stewart and Barber 2010); however James Bay is included in cartographic presentation.

The primary Region of Interest (ROI) is highlighted in Figure 3-1 (a) – the northwestern coastline extending from Cape Churchill to the southwest extremity of Southampton Island, there directly to the mainland coast. This does not include the Roes Welcome Sound – the body of water between the Nunavut mainland and Southampton Island – which is analyzed separately. This area approximates the modelled winter sea ice anomaly referenced in Saucier et al. (2004).

Table 3-1 - Geometry of Subregions.

Feature No.	Region	Area (km^2)	Centroid Longitude (°W)	Centroid Latitude (°N)
1	Central Basin	370,970.41	86.10	59.25
2	Southeast	77,668.06	78.48	57.81
3	Nelson Estuary	11,814.66	91.85	57.74
4	Roes Welcome Sound	11,442.16	86.68	64.81
5	Northwest Shore	77,769.62	91.62	61.49
6	Southampton Island	26,382.89	84.87	63.23
7	South Shore	49,290.76	85.44	56.15
8	James Bay	61,802.21	80.46	53.32
9	Coats Island	33,664.29	82.97	62.22
10	Mansel Island	22,807.57	80.15	61.95
11	East Islands	53,938.53	79.91	58.50

Manually-defined regions were used to segment the marine area for temporal analysis – a technique used in Etkin et al. (1990); Hochheim et al. (2011); Scott and Marshall (2010); Gagnon and Gough (2005b); Bareiss and Görgen (2005) and others. Regions were defined to agglomerate coastal areas with similar aspect or areas

surrounding islands. The choice of regions was not strictly *a priori* to the analysis: descriptive statistics, visual analysis of optical and passive microwave imagery, and a hypertemporal principal components analysis were incorporated into study region selection (Piwowar, 2008). This investigation focuses on the features of the Northwest Shore, the Central Basin, Roes Welcome Sound, the South Shore, and the Southeast.

3.2 Data Sources

3.2.1 Passive Microwave Orbital Data

The primary data source for this analysis is the Advanced Microwave Scanning Radiometer – Earth Observation System (AMSR-E) – a passive microwave sensor aboard the NASA *Aqua* satellite. This sensor has been demonstrated to reduce spatially-induced error, particularly in the case of ice edge and near-coastal areas of interest (Heinrichs et al., 2006). Operational from 2002-2011, this system provided the highest spatial resolution dataset (6.25 km) available to the passive microwave remote sensing community during this time period. AMSR-E Sea Ice Concentration data were obtained from the Centre for Marine and Atmospheric Sciences (ZMAW) at Hamburg and subset to the study area (Spreen et al., 2008).

3.2.2 Operational Ice Charts

To supplement Passive Microwave data, digitized data published as Canadian Ice Service Regional Ice Charts (CIS 2005) were leveraged to gain insight towards thickness and age distributions of the Hudson Bay ice pack. These data are considered high-level – individually produced as 'nowcasts' from a variety of data sources including orbiting

Synthetic Aperture Radar sensors, *in situ* thickness measurements and observations, aerial photography and photogrammetry, vessel reports, orbiting optical and thermal infrared sensors, and other supplemental data sources (CIS, 2005). The CIS technician produces a chart with surface polygons representing sea ice concentration (SIC), sub-polygon distribution of concentrations and floe size, stage of development (i.e. thickness), and forms of ice – called the Egg code. Archives of these charts are distributed online as ESRI Interchange (.e00) vector files, data was reprocessed as vector-based shapefiles and individual variables were converted to raster cells with 2.5 km spatial resolution.

The CIS Regional Ice Charts have been found to perform as well or better at discrimination of SIC than PMW (Agnew and Howell, 2003), and are used for sea ice climatologies of regions in the Canadian Arctic (Gagnon and Gough, 2005b; Galley et al., 2008; Hochheim et al., 2011). A significant benefit of the additional estimates within the Egg code is that a spatial distribution of ice thickness may be estimated (Ersahin et al., 2011). The low temporal resolution during winter months reduces the overall utility for analysis of rapidly-changing, short-term targets such as polynyas. Charts are only produced on a monthly basis from January to March, valid for 5 days prior to production (CIS 2006).

3.2.3 Optical Orbital Data

MODIS data were obtained as near-realtime, true colour regional subsets from the NASA Land Atmosphere Near-real time Capability for EOS (LANCE). Landsat Thematic Mapper (TM) data was obtained from the United States Geological Survey Earth

Explorer. Data were reprojected to the modified Albers Equal Area projection for consistent display using ESRI ArcDesktop 10.2 (Appendix 6.3)

Although remote sensing of winter sea ice using optical imagery is notoriously difficult (Lubin and Massom, 2006) due to low solar insolation during winter months and high cloud cover due to polynya/lead vapour flux, many optical sensors have long data archives and relatively high spatial and temporal resolution and are inherently straightforward to interpret. Data from the MODIS sensors on the *Aqua* and *Terra* satellites have a combined twice-daily nearly-global coverage at 250 and 500 m spatial resolutions. Landsat Thematic Mapper data is part of the thirty-year Landsat Archive: a 30 m spatial resolution dataset with weekly temporal resolution. These data allow, when surface conditions permit, a significant addition to case studies and identification of floe size. When presented as a static time slice optical data can present change over time and motion of sea ice (Larouche and Dubois, 1990).

3.2.4 Oceanographic Data

In situ oceanographic data was collected aboard the Canadian Coast Guard Icebreaker *Amundsen* on Leg 1a of the ArcticNet 2010 cruise (ArcticNet/Gratton, 2010). Conductivity, Temperature, and Depth (CTD) data were collected by the science crew with a Sea-Bird CTD/Rosette frame at predetermined stations. CTD probes were regularly validated against samples using an AutoSal 8400B. Data was plotted with Ocean Data View 4 and horizontally interpolated with DIVA – a finite element method for gridding appropriate for oceanographic data (Troupin et al, 2012).

3.2.5 Atmospheric Data

Gridded atmospheric data were obtained from the North American Regional Reanalysis (NARR/NCEP). This is a high spatial-resolution reanalysis of climate data over the North American continent with 29 pressure levels. Zonal and meridional winds – u component and v component respectively – at 1000 mb are used to gain insight to atmospheric forcing near-surface. Based on literature and aspect of the coastline in question, zonal winds will be the focus of the analysis.

Local Surface Air Temperature (SAT) data for proximal terrestrial stations (Churchill, MB; Arviat, NU; Rankin Inlet, NU) was provided by the Environment Canada Digital Climate Archive.

3.3 Analysis

3.3.1 Determination of Consolidated Period

For annual descriptive statistics, the year was quartered by calendar months following the convention for the Canadian Arctic – January February March (JFM); April May June (AMJ); July August September (JAS); and October November December (OND) (Hochheim et al., 2011; Tivy et al., 2011). Seasonal analyses were directly compared by using an Adjusted Date of Season (aDOS) which used the vernal equinox as a reference point to reduce calendar-based error (Cerveney et al., 2008). The numerical order for each winter season begins on or around September 1: reference dates can be found in §6.4.

Calculations of annual consolidation and ablation periods are made in to restrict the definition of 'polynya' to the period of predominantly consolidated regional ice. The

ice-covered period extends from the first date with no open water extent (pixels ≤ 15 % SIC) to the last date with no open water pixels.

3.3.2 Spatial and Temporal Analyses of Sea Ice and Atmosphere

Prior to analysis, data were reprojected from the custom Polar Stereographic projection to a suitable Albers Equal-Area projection with nearly zero pixel aspect rotation (see Appendix). This allows areal calculation of large regions with minimal projection-induced error. Reprojection used nearest-neighbour rules to eliminate alteration of the data due to averaging.

Passive microwave data from the AMSR-E ASI algorithm were not agglomerated into weekly or monthly averages as has been done in other studies of Hudson Bay sea ice climate (Spreen et al. 2008; Hochheim et al., 2011; Galbraith and Larouche, 2011; Scott and Marshall, 2010). The target phenomenon of this study – like many coastal polynyas – occurs on the daily- to weekly time scale precluding weekly or monthly groupings. To reduce error a conservative threshold was chosen and data were subsampled from an 8-bit resolution to a binary presence/absence map.

Review of Sea Ice Concentration Classes (SICCs) (Table 2-1) demonstrated a diversity of options in the selection of an ice presence/absence threshold. The principal analysis of this investigation uses the widely-accepted 15% SIC threshold as a demonstration of sea ice extent to remain conservative in estimates of polynya area (Heinrichs et al. 2006, NSIDC). Open water extent (OWE) is defined as the complimentary areal measure to sea ice extent (i.e. OWE ≡ Sum of Pixels ≤ 15%).

The passive microwave data was chosen to balance between the high spatial resolution and daily temporal resolution of the dataset. Initial analysis involved descriptive statistics applied to individual cells within their spatial context to produce seasonal normals and examine the nature of SIC variability. A Principal Components Analysis of spatially-gridded data was used to examine spatial distributions of positive/negative correlation during the consolidated period (Piwowar et al., 1998; de Beurs and Henebry, 2005; Piwowar, 2008).

With regions determined in §3.1, a zonal analysis was undertaken with the consistently projected gridded data using nearest neighbour selection rules. Cumulative counts and descriptive statistics for each region are calculated using Zonal Statistics as Table from ArcGIS 10.2 Spatial Analyst extension (Bareiss and Görgen, 2005). NARR gridded data was analyzed in a similar fashion to passive microwave data using identical zonal features.

The relationship between atmospheric and sea ice data was tested using a Spearman's Rank Correlation test: a nonparametric statistical test of relationship between paired variables. In this analysis the mean u-component vector of wind from NARR gridded data for the study area was compared with open water extent with no lag applied.

4 RESULTS AND DISCUSSION

4.1 RESULTS

Results are presented in the order of the three research objectives presented in §1.1. Before the full analysis, a definition of seasonal study periods is shown. The morphology — including size, shape, and presence of the sea ice anomaly in Hudson Bay is presented to demonstrate individual events and confirm the polynyas recurrent existence. The spatial and temporal recurrence, size distribution, and cumulative wintertime open water area are then presented. Relationship to hypothesized atmospheric forcing is then demonstrated. A single polynya opening event is examined in detail with a case study by presenting sea ice, oceanographic, and atmospheric data sources. Additional findings relating to the Hudson Bay sea ice regime are shown as a comparison to the northwest polynya region.

4.1.1 SEASONAL STUDY PERIODS

The polygon consolidated period was calculated to ensure seasonal ice congelation/melt effects were separated from polynya events by defining the period beginning as the first day with 0% open water extent (100% sea ice extent) and ending with the last day of 0% open water extent. Within this period variation in open water extent is presumed to be due to formation of polynya, rather than part of bay-wide ice formation or melt processes in the fall and spring respectively. This measure, called the polygon consolidated period, is used as the seasonal period of study for sea ice (Table 4-1).

Table 4-1 - Northwest Polygon Consolidated Period

Season	Beginning	End	Duration (days)
2003/2004	11/12/2003	09/04/2004	120
2004/2005	02/12/2004	29/04/2005	148
2005/2006	03/12/2005	13/04/2006	131
2006/2007	22/12/2006	06/04/2007	105
2007/2008	30/11/2007	16/05/2008	168
2008/2009	12/12/2008	21/04/2009	130
2009/2010	10/12/2009	27/04/2010	138
2010/2011	13/12/2010	08/04/2011	116

4.1.2 Northwest Hudson Bay Polynya Morphology

The polynya in Northwestern Hudson Bay exists (Figure 4-1). An analysis of the northwestern marine region demonstrates that during the winter period there is a large expanse of open water (SIC ≤ 15%) while the rest of Hudson Bay remains heavily or completely ice covered. During the entire study period mean polynya event open water extent (OWE) is 1,672 km^2 and median OWE is 820.31 km^2. Events range in size from the minimum mapping unit (39.06 km^2) to an observed maximum extent of 13,867 km^2 on March 17, 2010 (detailed in §4.1.5). Annual SIE event maxima range from 4,726 km^2 (2008/2009) to 13,867 km^2 (2009/2010), indicating a significant amount of interannual variability. Small open water extent values near the minimum mapping unit skewed the data towards the low end, however examination with SIC data demonstrates spatial features consistent with weak or small polynyas. The conservative threshold (15%) does not account for the full polynya size (i.e. total disturbed area); although it does create a distinction between periods with significant open water and brief openings (Figure 4-2). Individual observations indicate an ice margin that

ranges from a distinct edge to a highly-fractured zone of marginal ice, with leads reaching deep into the pack.

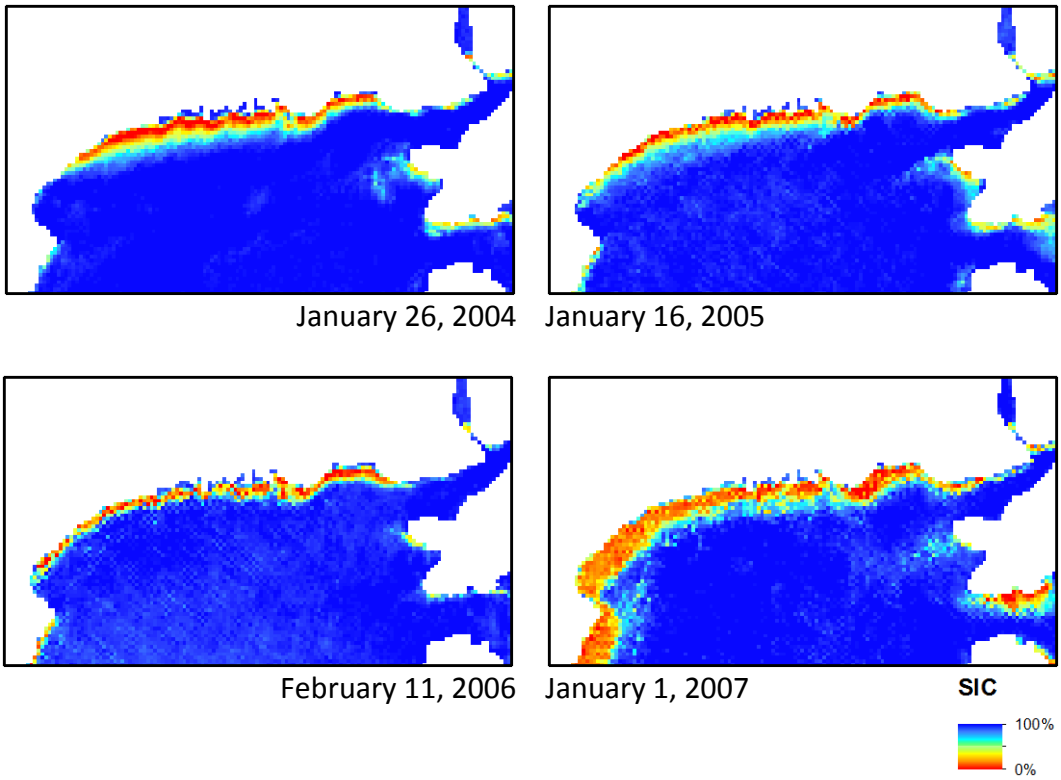

Figure 4-1 - Examples of Polynya Maxima

Typical length of opening is a 1-5 days with a defined peak (e.g. December 30, 2009); however there are instances during which polynya maintenance mechanisms keep a relatively constant size for up to 5 days (January 20-25, 2008). Polynya opening and closing are on similarly rapid time scales.

Spatial extent of the polynya using the SIE threshold falls entirely within the *a priori* zone polygon: results for the central basin (Figure 3-1(b), Region 1) maintain 100% SIE during winter over the study period. This emphasizes that open water periods to not extend into the central

basin during the study years and the region of interest encompasses the complete study area. Inspection of singular events shows major occurrences (>2 pixels) open water areas are close to each other and the coastline, supporting the connection between low SIE and polynya events.

Distribution of polynya susceptibility can be seen for the entire basin in Figure 4-6. Mean SIC (a) demonstrates a trend of potential disturbance across the entire coastline of the bay and around islands, particularly the Belchers and Southampton. Figure 4-6 (b), the minimum statistic, demonstrates the area that experiences low-to-very low SIC at least once during the overall study period. A large area on the east coast of the basin opened during a single event (§4.1.6). Visual comparison between Figure 4-6(a) and (c) shows statistical distribution of low SIC: the median is at or near 100% SIC for most of the bay with only a few coastlines with more frequent openings. Highest local values for the mean u-component of wind during JFM are found in the southern half of Hudson Bay, with high (westerly) winds across most of the bay (Figure 4-6(d)). This is consistent with a prevalent low pressure system described in §2.3.3.

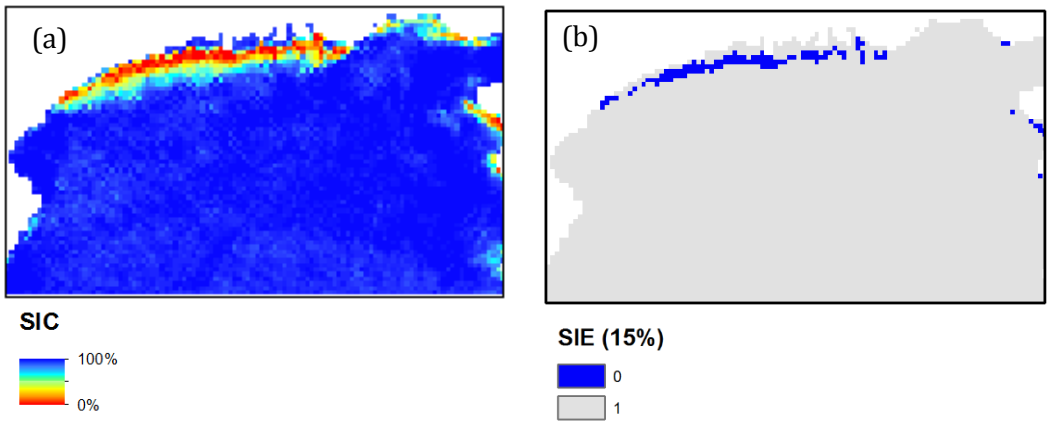

Figure 4-2 – Same date comparison of SIC (a) to SIE (b) – March 4, 2008

Examples of spatial distribution of SIC during polynya events are displayed in Figure 4-1. All events displayed occurred following a complete SIE coverage of the northwestern polygon. Typical of polynya openings are a gradient in SIC values moving offshore, with a small width (~2 pixel, 12.5 km) of presumably fast ice from the ASI landmask, a region of 0% SIC, followed by a gradient of increasing ice concentration farther offshore. In nearly every event there are associated large areas on the east coast of Southampton Island with low ice concentration, further supporting the atmospheric forcing hypothesis for polynya formation and maintenance.

Width of the feature from shore appears uniform along the coastline, although the total length of the polynya may not include the entire west coast (e.g. Figure 4-1 January 26, 2004). Observed measurements of full polynya width – fast ice margin to 100% SIC – exceed 50 km (31 miles) in the largest events. In the January 1, 2007 event the consolidated ice pack appears to hold the shape of the coastline as the pack appears to be forced offshore.

The primary domain of this polynya extends from north of Cape Churchill to the mainland directly across from the southwestern extremity of Southampton Island; from the variable fast ice margin in the west to a line offshore dependent on forcing. The Roes Welcome Sound rarely presented a large open water extent (maximum observed: 1,328.13 km^2); often forming the northern limit of the northwestern polynya (detailed in §4.1.7).

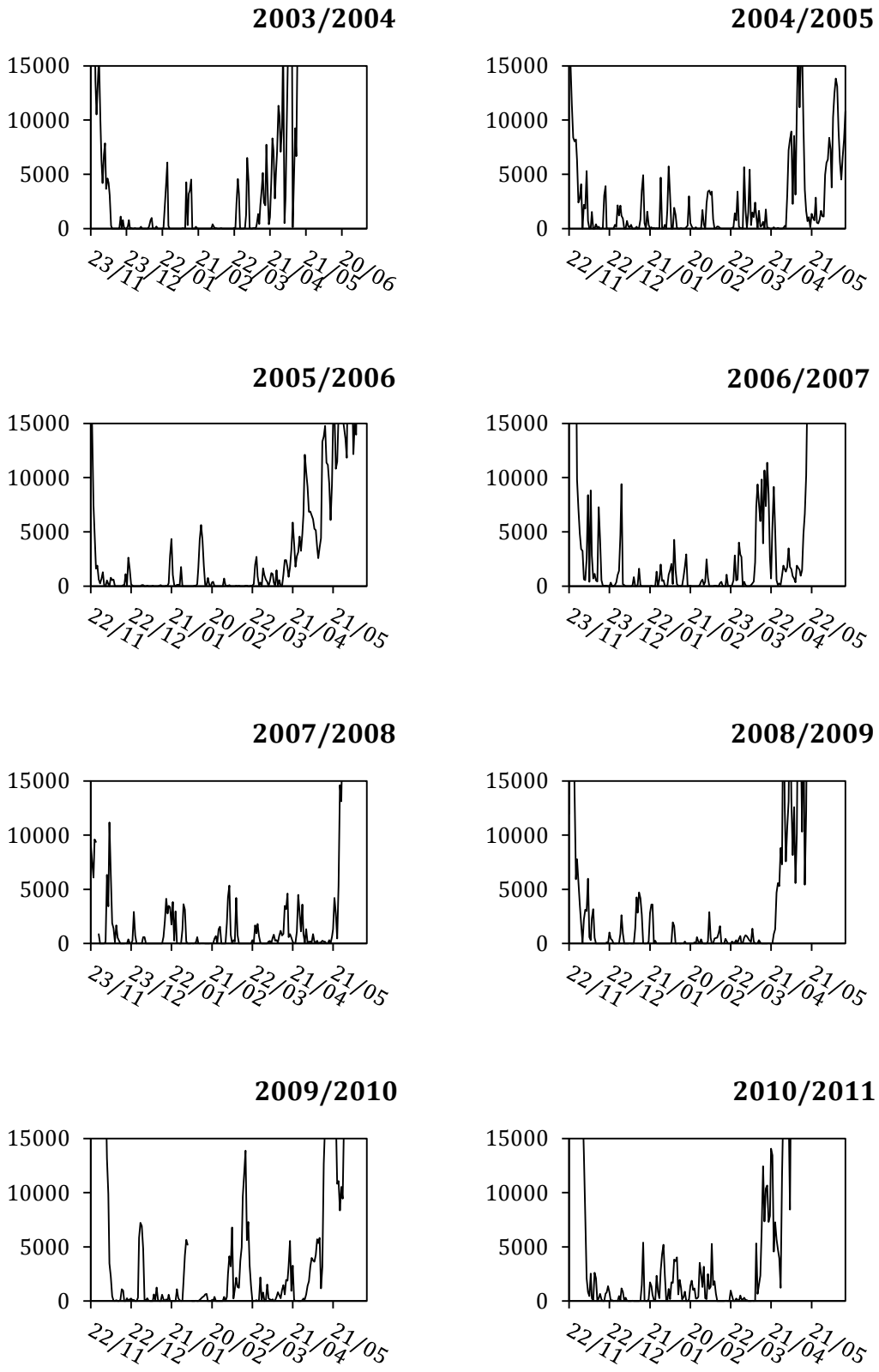

Figure 4-3 - Sea Ice Extent in Northwestern Hudson Bay (Region 5).

Table 4-2 - Descriptive Statistics of Polynya Events

	2003/ 2004	2004/ 2005	2005/ 2006	2006/ 2007	2007/ 2008	2008/ 2009	2009/ 2010	2010/ 2011
Count	27	49	42	29	58	38	47	43
Mean (km^2)	1,734.7	1,888.6	1,064.9	1,472.3	1,729.5	1,216.1	2,419.4	1,627.9
> 2 pixel Count	19	43	27	22	48	32	43	35
> 2 pixel Mean	2,446.5	2,143.9	1,627.6	1,928.3	2,080.9	1,436.8	2,639.0	1,988.8
Largest Event (km^2)	6,523.4	5,742.2	5,625.0	9,414.1	11,171.9	4,726.6	13,867.2	5,390.6

4.1.3 Spatial and Temporal Variability of the Polynya

To understand variability and quantify opening and closing events a time series was created for the polygon discussed in §3.1. A polynya event is defined as a temporally contiguous period where open water area is greater than zero. Seasonal time series are displayed in Figure 4-3 from late November to late May. There is no discernable intraseasonal signal beyond formation and melt events. Seasonal mean open water extent ranges from 1,064.9 km^2 in 2005/2006 to 2,419.4 km^2 in 2009/2010 (Figure 4-5(a)). Seasonal event counts (with each event defined as a period of open water between periods of entirely closed water) range from 27 during the 2003/2004 winter season to 58 in the 2007/2008 winter season (Figure 4-5(b)). This variation appears related to infrequent long periods of open water rather than an overall increase in size. No trend in polynya size or frequency was observed during the study period.

Size/frequency relationships are plotted on a duration exceedance chart (Figure 4-7). Relationship between size and duration over the consolidated portion of the season is roughly

logarithmic in each year, however there is suggestion of two distinct patterns. Certain seasons (2004/2005, 2007/2008, 2009/2010, 2010/2011) demonstrate higher frequency of small open periods while 2003/2004, 2005/2006, 2006/2007, and 2008/2009 have significantly fewer small openings. All seasons converge in frequency of openings greater than 4,000 km^2.

This seasonal division is also observed in cumulative open water extent. Sum of total open water extent shows two distinct groups: those with low but consistently similar cumulative extents (2003/2004, 2005/2006, 2008/2009), and those with much higher cumulative extents (2004/2005,2007/2008, 2009/2010). With the exception of 2010/2011, the seasons with higher cumulative extents also have more frequent small openings.

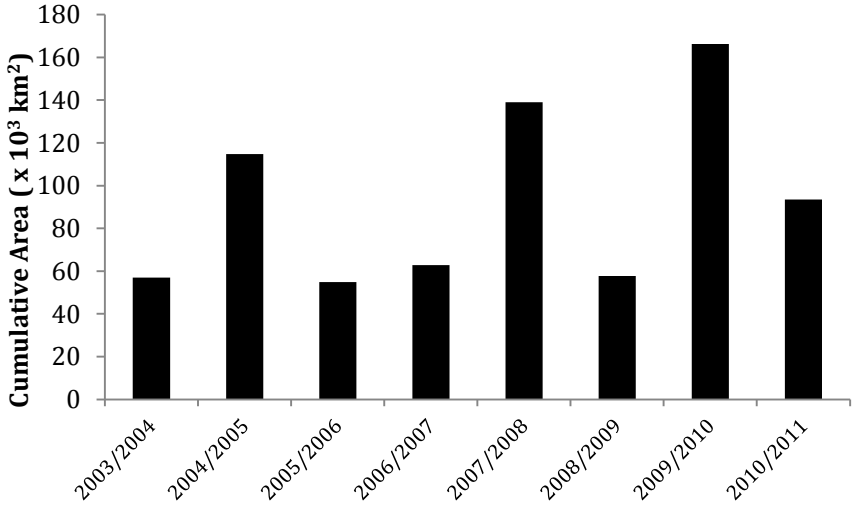

Figure 4-4 – Seasonal cumulative open water extent in Northwest study area

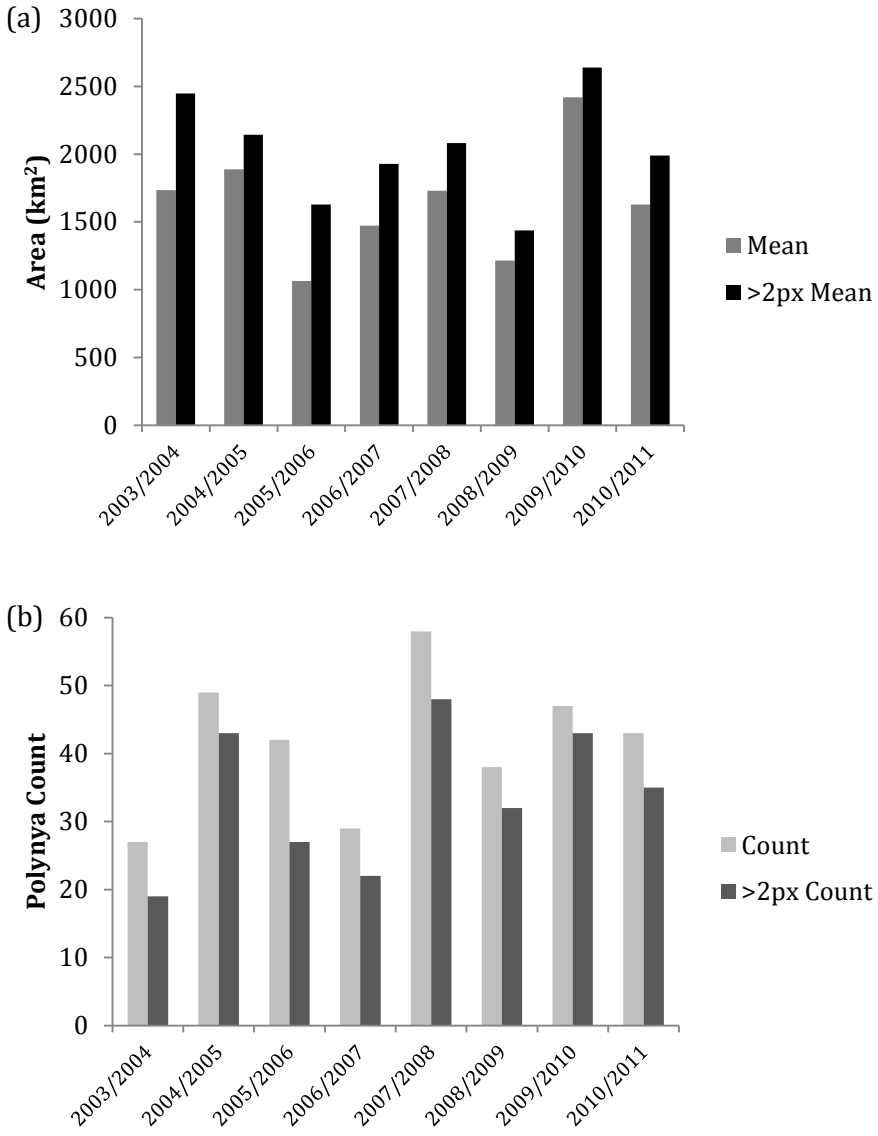

Figure 4-5 - Mean Polynya SIE (a) and Count of separate open water events (b)

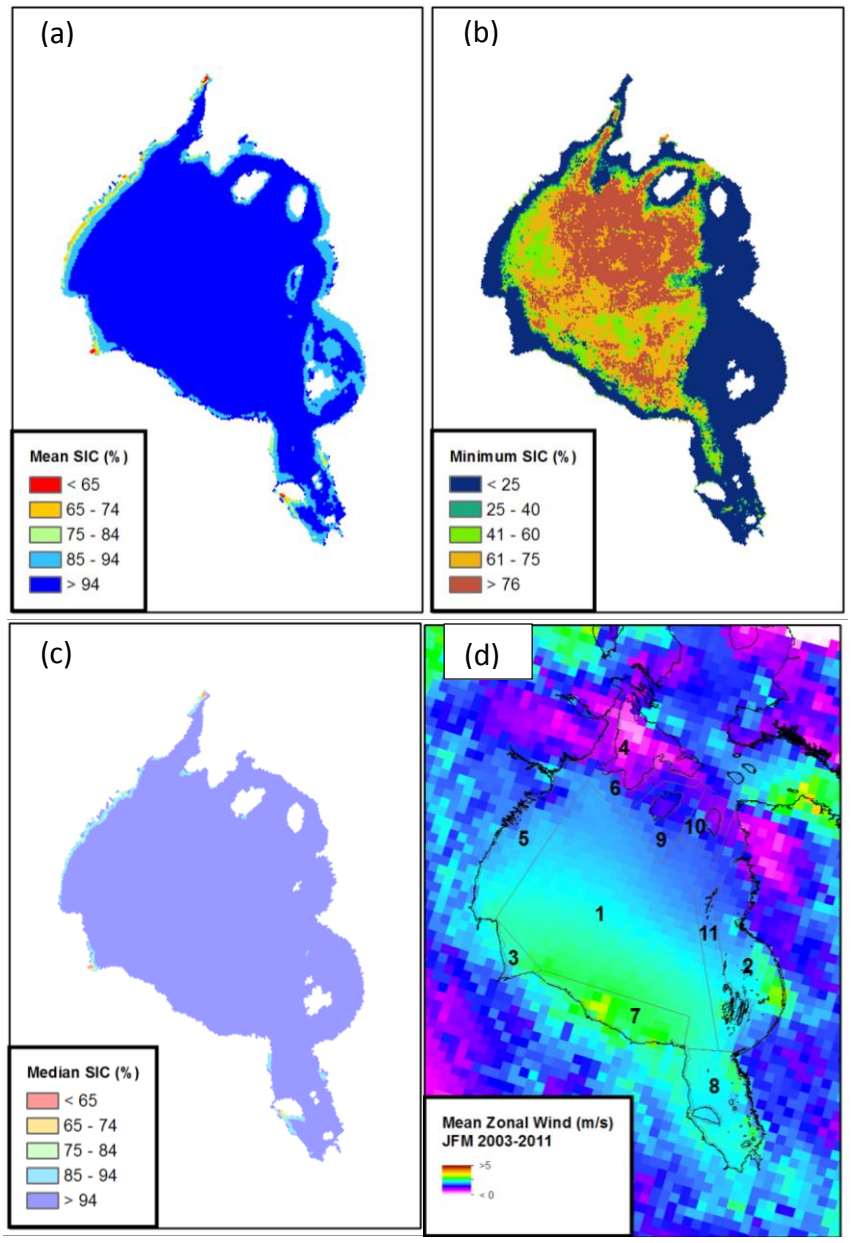

Figure 4-6 - Descriptive Statistics for January, February, March 2003 – 2011.
(a) Mean; (b) Minimum; (c) Median; and (d) Mean Zonal Wind.

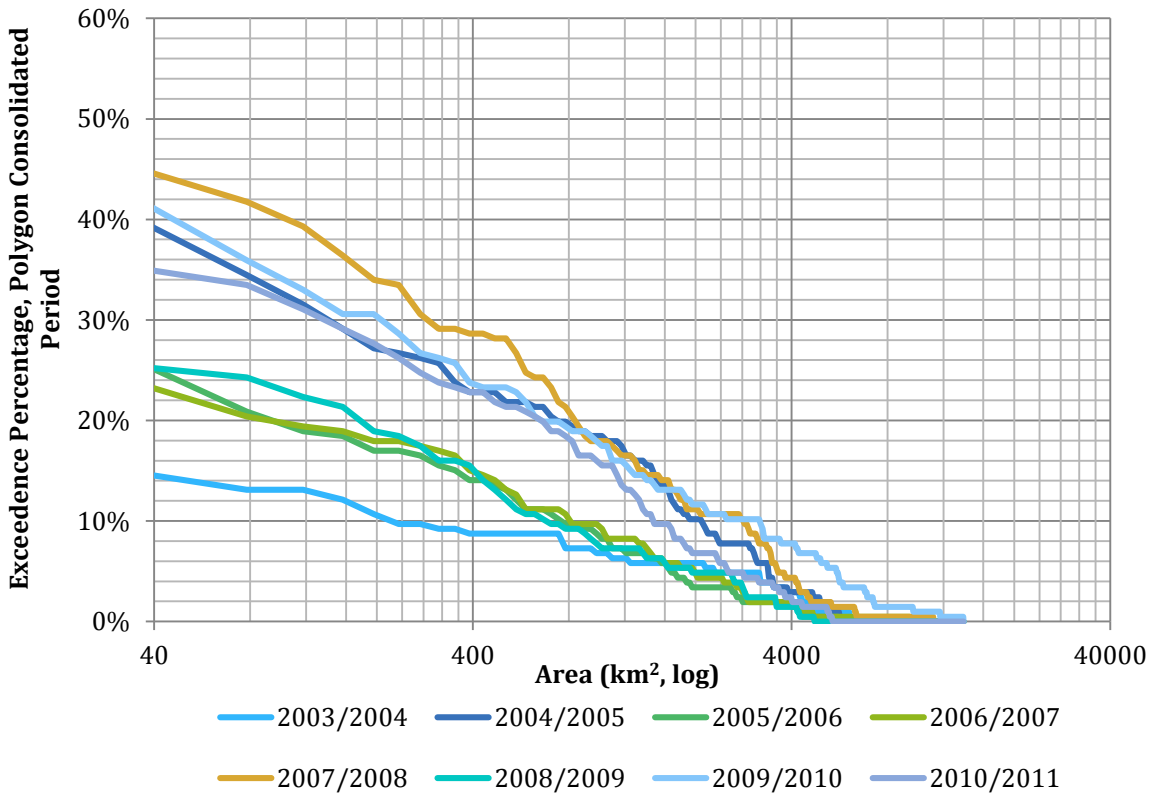

Figure 4-7 – Percent of consolidated period of open water extent

Table 4-3 - Spearman's Rank Correlation between OWE and U-Wind

	2003/ 2004	2004/ 2005	2005/ 2006	2006/ 2007	2007/ 2008	2008/ 2009	2009/ 2010	2010/ 2011
ρ	0.565	0.471	0.396	0.599	0.518	0.534	0.394	0.488
n	121	149	132	106	168	131	139	117

4.1.4 Atmospheric Forcing Mechanisms

This case study is presented to examine in detail a single event of the polynya opening with multiple data types. An examination of atmospheric forcing was conducted by comparing open water extent to the zonal component of winds at the 1000 mb pressure level from the North American Regional Reanalysis dataset (NARR/NCEP). A Spearman's rank correlation (ρ) was chosen because of the nonparametric nature of the data and observed monotonic relationship of the paired datasets. The null hypothesis (H_0) was no relationship between zonal winds and open water extent. The test statistics for each season are reported in Table 4-3, all of which exceed the critical value for a t-distribution with $p \leq 0.01$. This indicates H_0 may be rejected at the 99% confidence level. This observed relationship between local near-surface winds and open water extent support model results regarding local forcing mechanisms (Saucier et al., 2004).

4.1.5 March, 2010 Event Case Study

The largest polynya observed reached a peak open water extent (OWE) of 13,867 km^2 on March 17, 2010. Polynya morphology at maximum is a non-linear region north of Cape Churchill, at the south end of the study polygon (Figure 4-12). A concurrent polynya event occurs in the Nelson Estuary, both polynyas briefly are connected at maximum in a pattern seen occasionally with large polynya openings (similar to January 1, 2007, Figure 4-1). The following section describes the periods before, during and after the event to gain insight into forcing and maintenance mechanisms of this feature.

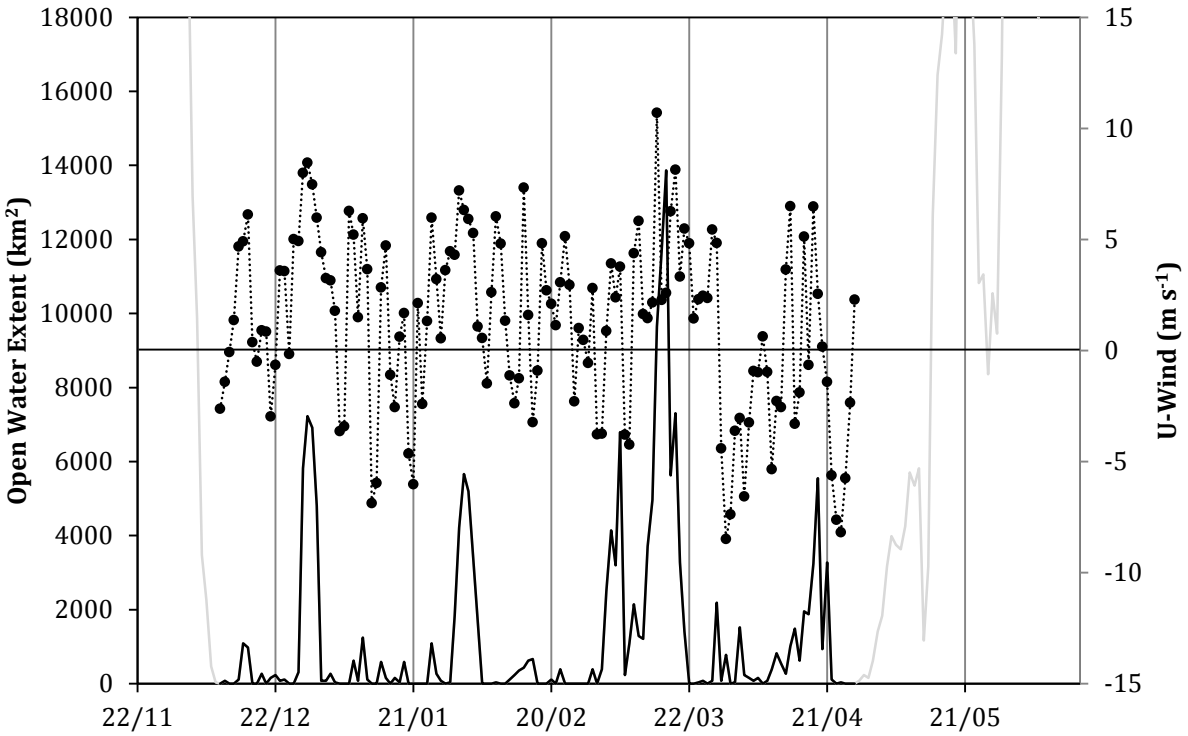

Figure 4-8 - Measured Open Water Extent (solid black) and Mean U-Wind (dashed with points), Northwestern Polygon. OWE outside of regional consolidated period is displayed in light grey.

The consolidated period began following a rapid decline in OWE, reaching 0% on December 10, 2009. Rapid decline in OWE likely indicates *in situ* ice formation rather than extra-regional ice advection, typical to consolidation patterns in the observed years. Wind data show westerly winds for the first five days after consolidation, with a shift to easterlies on the date the ice formed. Complete coverage lasted four days until the wind again shifted offshore, creating a small open water extent and large area of low SIC in the young ice pack. Data from this time period indicates a large open water area on the East side of the bay, still unfrozen.

Prior to the event of interest there were two large openings: one peak on December 30 with a maximum OWE of 6,914 km^2 and other on February 2 with OWE of 5,195 km^2 (Figure 4-8). Both events are coincident with positive zonal (i.e. westerly) wind values: u-wind for the

first event peaked two days before the sea ice, maintaining a positive value until after the OWE had declined to 78 km^2, or the area of two AMSR-E pixels. The decline in wind appears to be associated with OWE declining rapidly, however this event does not indicate forcing mechanisms closing the polynya are negative zonal (easterly) winds, rather that the decline in dynamic forcing was not able to move the ice enough to counteract ice growth due to heat flux (Pease, 1987). The second large opening event of the season follows this pattern: a large sustained positive zonal (westerly) value, which declines and causes a rapid reduction of OWE.

This pattern becomes apparent in the large event of March 17, 2010. On February 27, ice completely covers the region. U-wind components are negative or in the low positives from February 25 to 28, imparting little momentum into the pack. On March 1 there is a slight mean westerly wind over the polygon and a narrow coastal polynya opens, but closes once the wind declines below its maintenance threshold.

The major event of March 2010 has two peaks days of OWE. The first reaches its maxima on March 7 at 6797 km^2 (Figure 4-9(b)). Forcing for this event appears to be the positive zonal winds, which last until the day of the maxima. On March 8, the 1000 mb winds shift to an easterly direction and the OWE responds by declining to 234 km^2 – a rapid and considerable decline in area. Optical imagery indicates this decline can be explained as both movement of the ice pack and frazil ice growth on the open water area (Figure 4-9(c)).

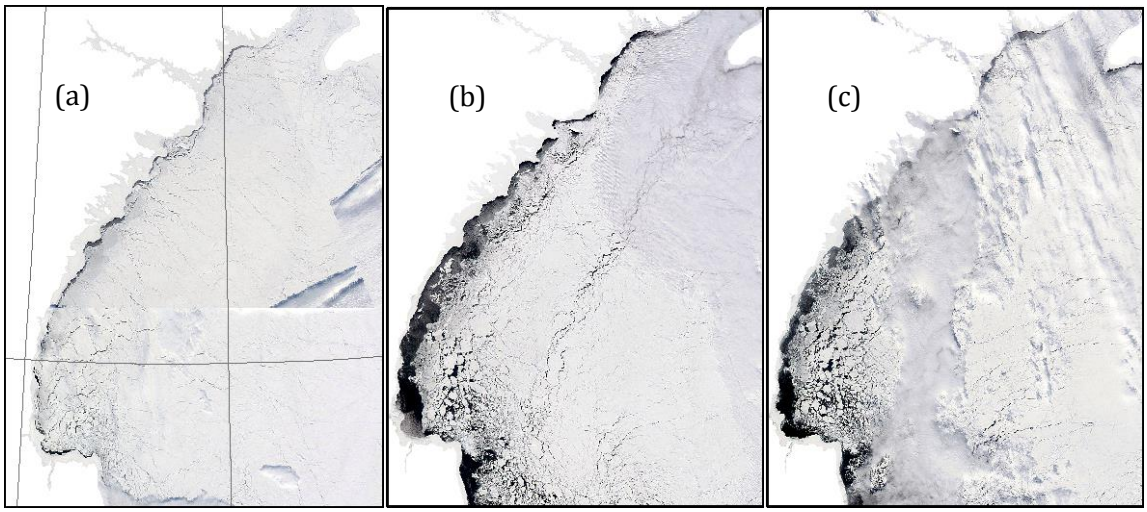

Figure 4-9 - Composite of MODIS True Colour Images – February 27/28, 2010 (a); March 7, 2010 (b); and March 8, 2010 (c).

On March 10 winds at 1000 mb once again return to a positive zonal component, suggesting a new opening phase may begin. Vector winds during this are demonstrated at this time in Figure 4-10. Winds are highly consistent across the Hudson Bay marine area. Surface air temperature from Environment Canada climate stations in coastal communities is presented in Figure 4-13, indicating stable temperatures at all three stations during this formation period between -10°C and 0°C.

With formation mechanisms in place, the largest observed polynya event reaches maximum on March 17, 2010 (Figure 4-12). This polynya has an atypical morphology, with very little open water on the northern portion of the coast and a large, non-linear open water area north of Churchill, MB. Ice fog and cloud cover are apparent downwind of the polynya (Figure 4-12(a)).

Within six days of March 17 open water extent returned to zero. This decline cannot be explained by zonal winds or general wind vectors (Figure 4-11). Rather it is apparent that surface air temperatures decreased drastically immediately following the polynya maximum

(Figure 4-13). Vector wind data supports this, indicating an Arctic cold front moving in from the northwest. Significant heat flux from the rapid decline in SAT, rather than reduction in atmospheric momentum transfer, appears to be the cause of the polynya closing.

Figure 4-12 demonstrates true colour and ASI algorithm SIC on the date of polynya maximum: March 17, 2010. A large, non-linear feature forced by southwesterly winds opens extending from Cape Churchill up the coast. A second polynya is apparent south of this in the Nelson Estuary, suggesting some of the forcing is due to meridional (v-component) wind vectors as well as the measured zonal wind. This peak opening, 13,867 km^2 measured OWE, demonstrates little transitional ice concentration values and a clear boundary between the nearly consolidated central ice pack and the open water adjacent to the coast.

Figure 4-14 shows the impact of this rapid cooling on the open water area. Thermodynamic forces, in this instance, appear to rapidly produce frazil ice on the affected area. The PMW demonstrates sensitivity to young ice as increasing SIC. By March 23 – six days after the open water maximum – the northwestern study polygon will report zero open water. NARR gridded zonal winds do not report any negative values in this time period, demonstrating the polynya closing is thermodynamically-forced.

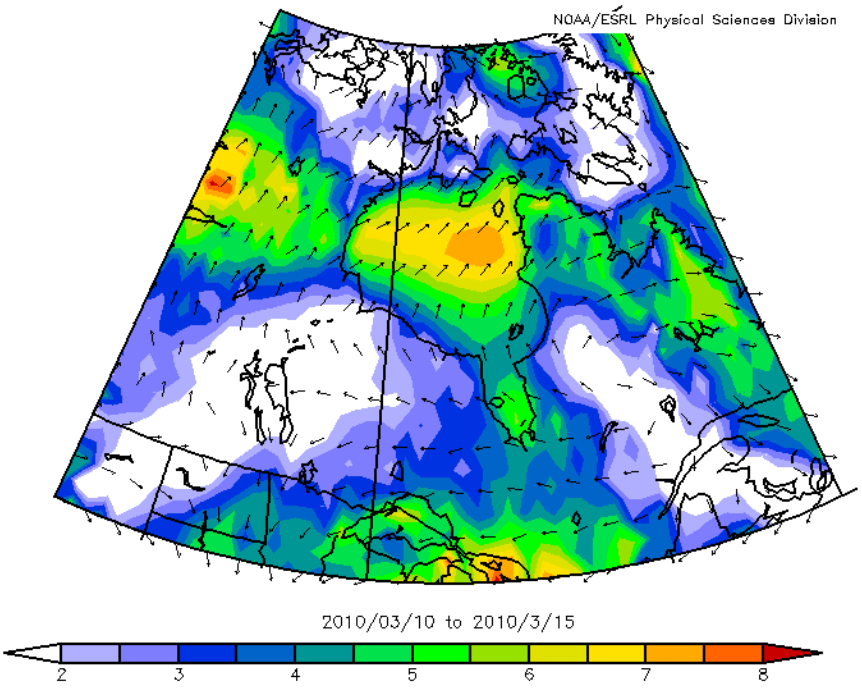

Figure 4-10 – NARR Vector Winds at 1000 mb pressure level (m s^{-1}).

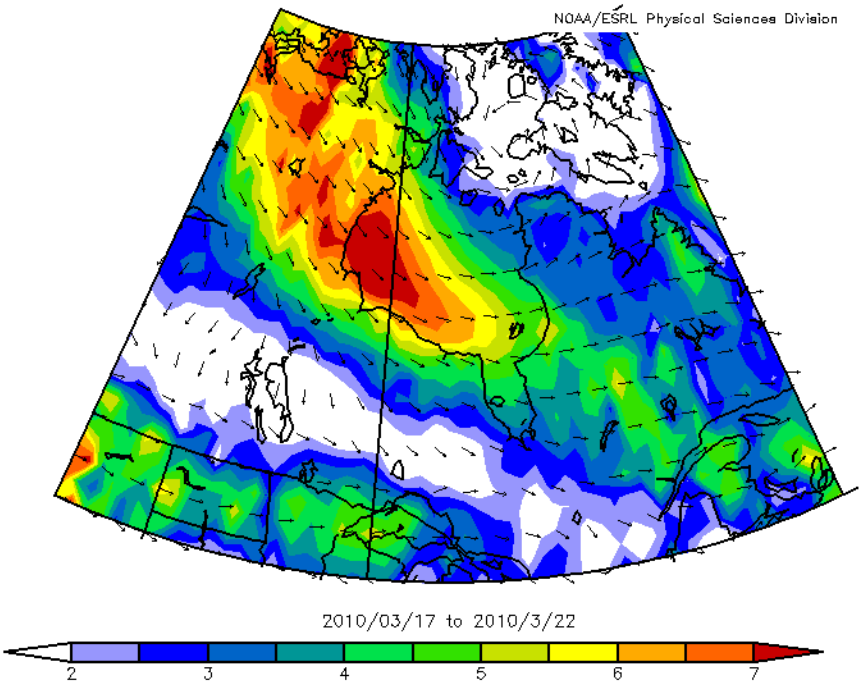

Figure 4-11 – NARR Vector Winds at 1000 mb pressure level (m s^{-1}).

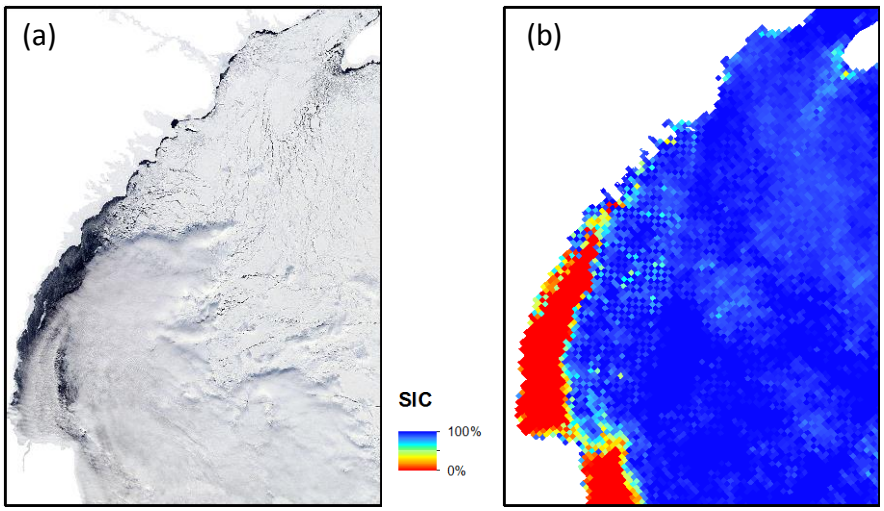

Figure 4-12 – MODIS Terra True Colour (a); and AMSR-E SIC (b) acquired at polynya maximum, March 17, 2010

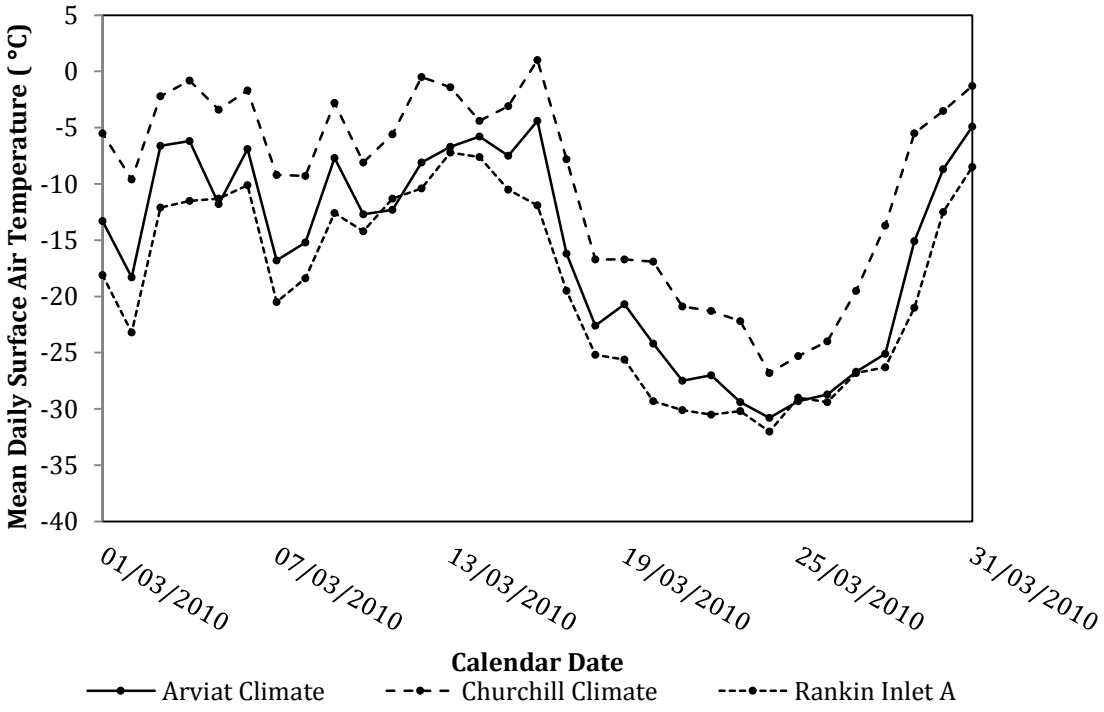

Figure 4-13 - Surface Air Temperature from coastal communities.

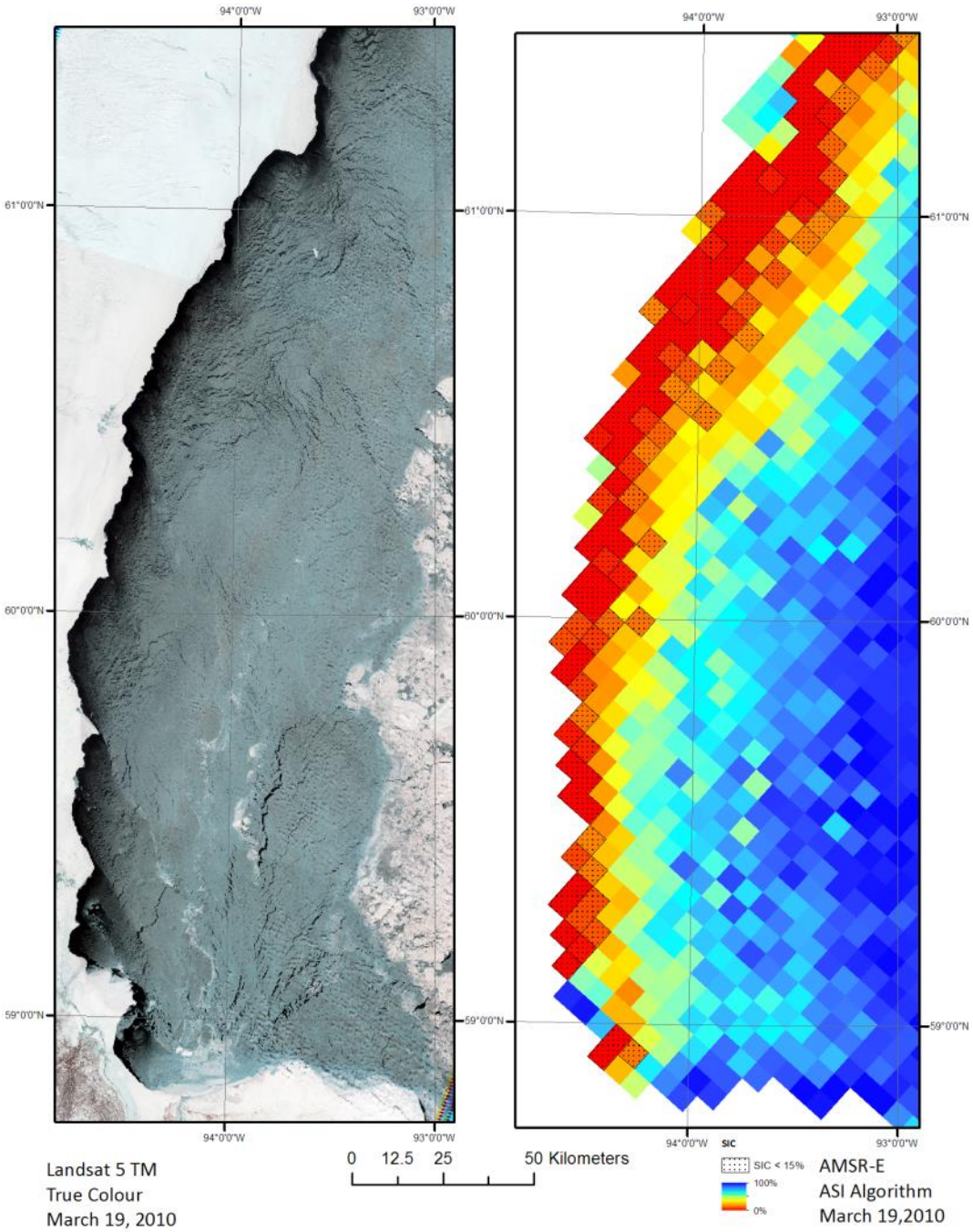

Figure 4-14 – Landsat TM True Colour Composite and AMSR-E SIC two days after peak open water extent

4.1.6 Significant East Coast Opening Event

The Passive Microwave data record demonstrates occasional anomalies along the eastern coast of Hudson Bay. Three events of significant sea ice extent decline took place in the early spring 2004, 2006, and 2009. In each event local ice declined in mid-April due to atmospheric forcing, from nearly complete ice coverage (~77,500 km^2) to below 50,000 km^2, a 35% decline in SIE. Events in 2006 (minimum of ~43,600 km^2) and 2009 (~48,000 km^2) were especially significant. Although not lasting more than a matter of days, these outlying events appear in spatial descriptive statistics (Figure 4-5 (b); Figure 4-16 (b); and Figure 4-17 (b)). During each the influence of atmospheric forcing is visible (e.g. Figure 4-15) as multiple blocking structures (shoreline, fast ice, islands) are adjacent to open water areas at a similar aspect angle.

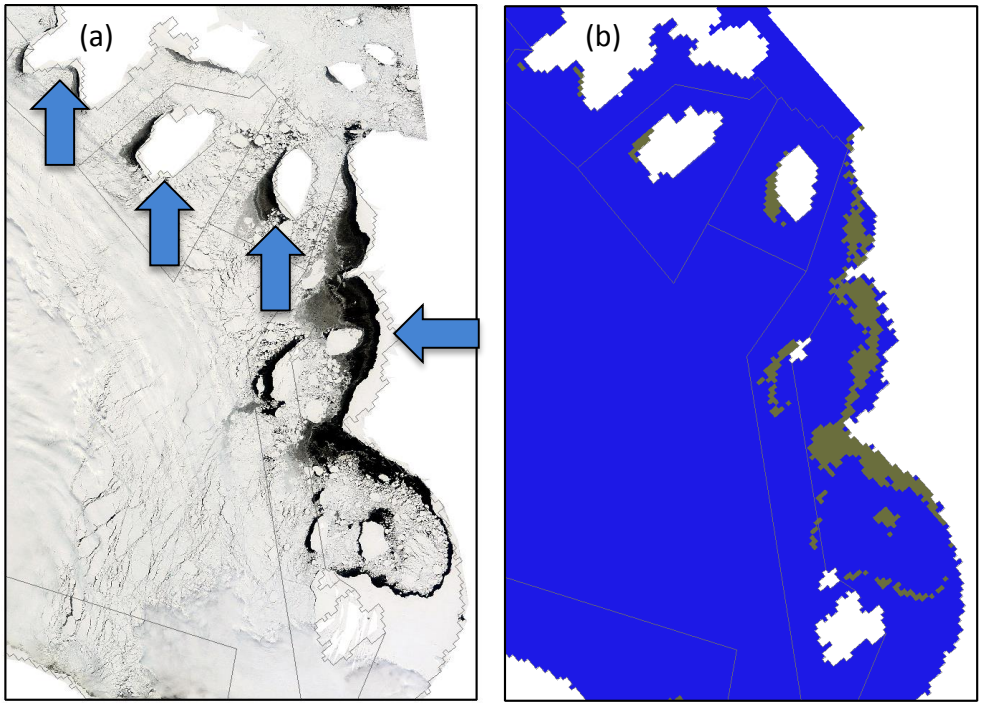

Figure 4-15 – (a) MODIS *Terra* Composite and ASI PMW 15% Threshold (b) April 15, 2009. Arrows coincident aspect in open water formation

4.1.7 ROES WELCOME SOUND POLYNYA

Maps depicting polynyas in the Canadian Arctic often note the shore lead system in Hudson Bay in addition to a large polynya formed in Roes Welcome Sound (Danielson, 1971; Smith and Rigby, 1981; Stirling et al, 1981; Markham, 1986; Barber and Massom, 2007). This investigation, through winters 2003/2004 to 2010/2011, did not observe a persistent polynya or lead system in this area. During part of the consolidated season, only one large open water event was observed: March 13, 2005 (aDOY 194). Open Water Extent (OWE) measured 2,890.625 km^2 in the polygon (refer to region 4, Figure 3-1(b)). Spatial distribution of this event was localized to the western coast of Southampton Island, as part of what appeared to be an atmospherically forced event. There does not appear to be a recurring pattern of opening, especially compared to the large northwestern coast polynya to the south. Smaller events occasionally occurred at the north end of Roes Welcome Sound, on the order of dozens of square kilometers.

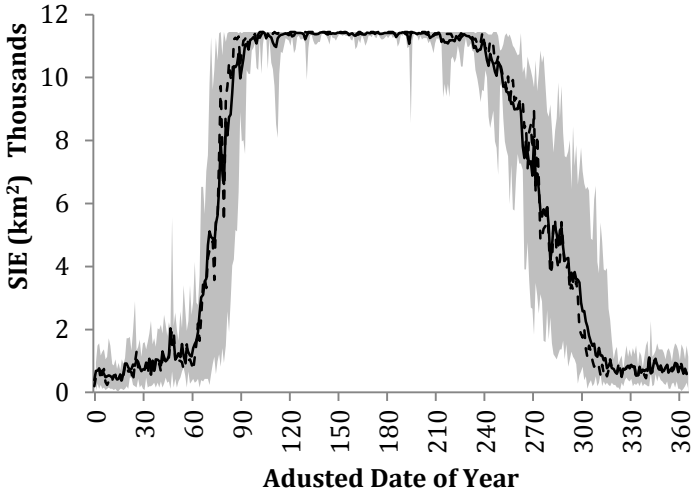

Figure 4-16 - Descriptive Statistics of Roes Welcome Sound Polygon (Region 4).
Dashed lines indicate median SIC, solid indicates mean, grey field indicates observed range 2003-2011.

4.2 DISCUSSION

4.2.1 HUDSON BAY COASTAL POLYNYA SYSTEM

Results presented above find the Hudson Bay coastal polynya system is large and complex. Although this study focuses on the northwestern polynya in Hudson Bay, it is part of a greater system of related sea ice anomalies. Figure 4-17 presents mean, median, and the range of observed SIE from the PMW dataset for the study period. Spikes in range above and below the central tendencies indicate single observed events – demonstrating the potential for variation at different parts of the year. Variability in the central basin is limited to formation and breakup periods: during the winter months the median and mean are consistently at the full extent of the polygon with nearly zero dispersion about the central tendencies. This implies that little of the overall variation in SIE is localized to the central part of the Hudson Bay basin.

Variation in extent during freezeup is concentrated in the northwest and southeast polygon. Freezeup begins in the southeast polygon over a range of thirty days, from aDOY 96 to aDOY 127 (approximately December 6 to January 6). In contrast, the central basin freezeup is only about two days in range. During the winter months when the southeast is consolidated, opening events tend to be infrequent, but large (§4.1.6).

To explore the relationship between sea ice concentration anomalies, a principal components analysis was applied to data from the central winter months; January, February, and March (Figure 4-18). When used on a long time-series dataset, principal components analysis rotates the data, performing an empirical orthogonal function to reduce dimensionality (Piwowar and LeDrew, 1995; Dragon et al., 2014). In the first principal component there is a highly negative correlation between the central pack and the shore (Figure 4-18(a)).

Unsurprisingly the greatest diversity of SIC during the winter months is localized to the coastal margin of the bay, where the coastal polynya system is located. The second principal component (b) demonstrates the very large opening types discussed in (§4.1.6).

The third and fourth components demonstrate the negative correlation between coastal ice anomalies during the winter months. Principal component 3 shows this negative correlation between the northwest study area and coasts with opposing aspects, with the exception of the southeast opening events. Principal component 4 demonstrates a similar north-south coastal opposition of SIC anomalies. This relationship between opposing coasts during the consistently consolidated months demonstrates that the motion of the Hudson Bay ice experiences forcing mechanisms that can move the entire sheet as a unit. This supports previous investigations that postulated an east-west asymmetry in atmospheric forcing and ice response (e.g. Gough et al., 2004a; Hochheim et al., 2011; McGovern, 2013). With few exceptions, when there is open water on one coast the facing coastal margin will be ice covered. This supports findings in both the models (Saucier et al. 2004) and observations of seasonal ice formation and melt (Saucier et al., 2004; Hochheim and Barber 2010; Hochheim et al., 2011).

While there is observed diversity along all coastlines, the northwest coast of Hudson Bay has the strongest, most persistent signal of a coastal polynya each season. Analysis of sea ice data and atmospheric data supports the hypothesis of this coast forming the large anomaly described in Saucier et al. (2004).

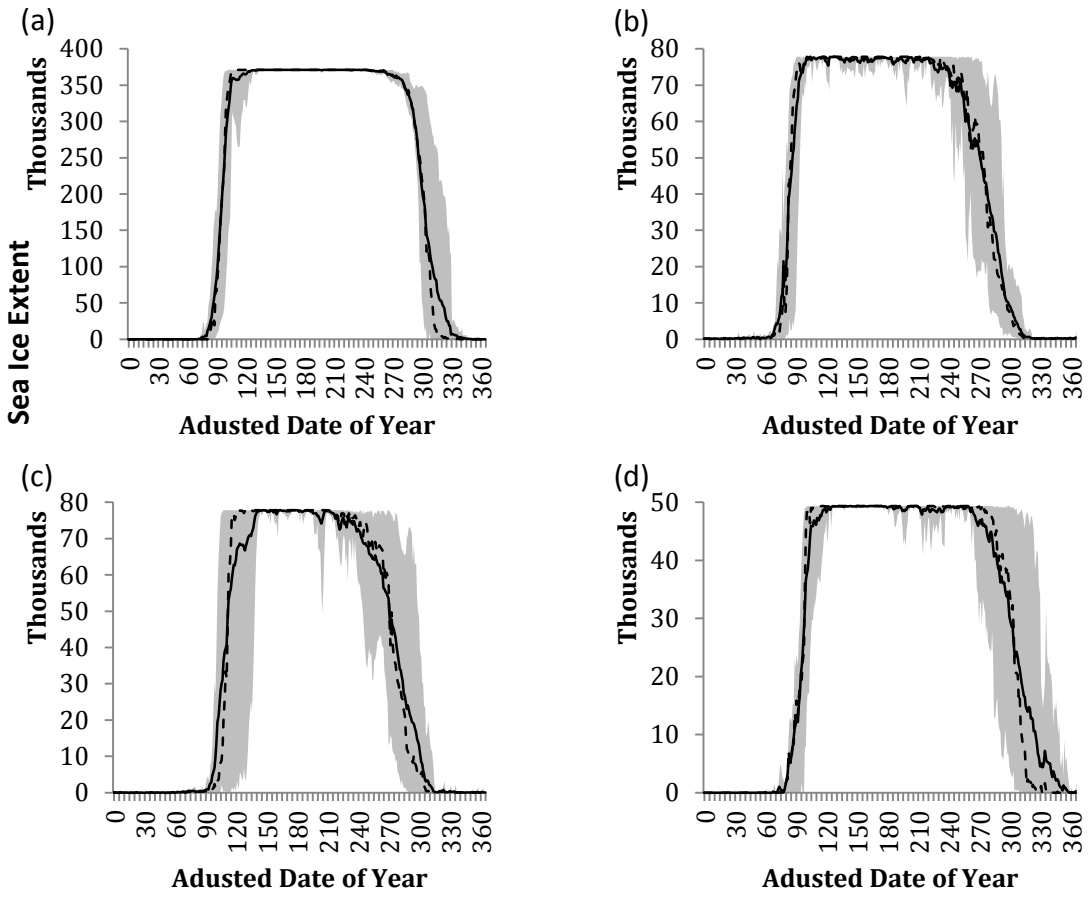

Figure 4-17 Annual Sea Ice Extent (a) Central Basin, (b) Northwest Coast, (c) Southeast, and (d) South Coast. Dashed lines indicate median SIC, solid indicates mean, grey field indicates observed range 2003-2011.

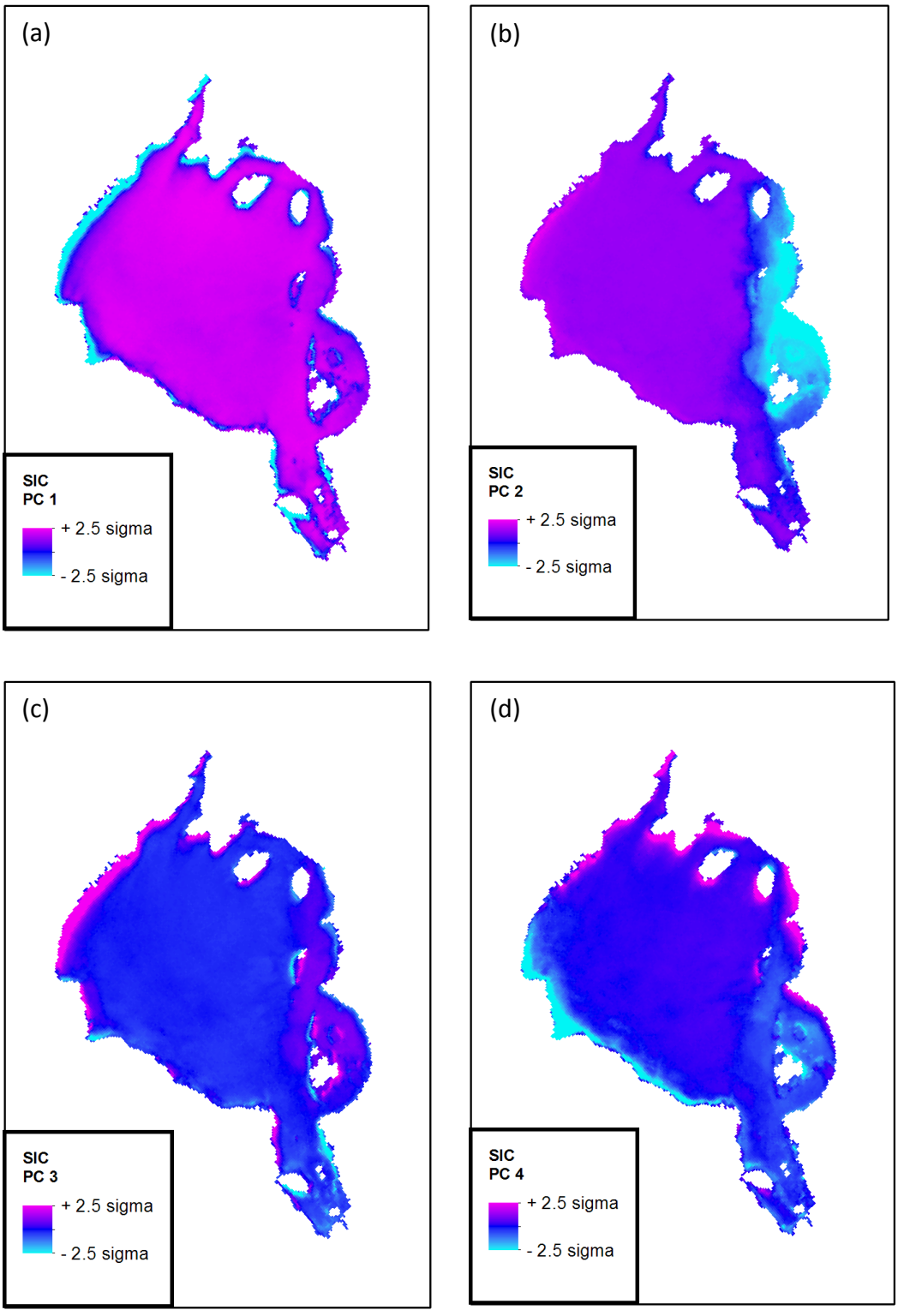

Figure 4-18 - Principal Components JFM 2003 – 2011. Eigenvalues in Appendix 6.5.

4.2.2 Atmospheric Forcing Mechanisms

The relationship between polar and midlatitude airmasses during the winter is changing (Francis and Varvus, 2012; Tang et al., 2013; Overland, 2014). The Hudson Bay Marine Complex and surrounding bodies of water are at the margin between polar and temperate air: so that these changes are likely to affect systems at the ocean sea ice atmosphere interface.

The coastline of interest is slightly curved along a south-north path, with an east-facing aspect. Coastal topography of this area is minimal: the rocky shores and headlands of this region are not likely high enough for orographic or katabatic atmospheric effects (Martini,1986). This coastline is roughly perpendicular to the prevailing geostrophic winds, which are dominantly from the west (Figure 4-6 (d)).

There is a demonstrated relationship between the zonal component of near-surface winds and winter open water area on the coast. These winds are influenced by hemispheric, synoptic, and mesoscale systems. To explore this relationship, data from the National Centers for Environmental Prediction (NCEP) Reanalysis is plotted to display correlational relationships between spatially-gridded climate reanalyses and climate indices (Figure 4-19, Figure 4-20).

The Arctic Oscillation (AO) and Southern Oscillation (SO) are key candidates for proxy measurement and teleconnection forcing of westerly winds on the western coast of Hudson Bay (Thompson and Wallace 1998; Parkinson et al. 1999). Correlation between the AO and the regional zonal winds is >0.4 in the northwest polynya region, indicating a degree of relationship (Figure 4-19). This agrees with the positive AO characterization of stronger midlatitude zonal winds and a distinct, high-latitude boundary between polar and midlatitude airmasses. The North Atlantic Oscillation, discussed in the literature review, was investigated and demonstrates a similar relationship to the AO. These oscillations are known to be highly

correlated (Ambaum et al., 2001). More than other coastlines in the region, the west coast of Hudson Bay is situated at the aspect and latitude to experience persistent westerly (positive zonal component) winds.

Mesoscale patterns impacting ice motion in Hudson Bay also include the recurrent Baffin Island low pressure system (Maxwell, 1986). This is described as strong system during winter months, weakening in the summer. This system, when centralized over southern Baffin Island, directs winds cyclonically with the system's southwest margin directly over the west coast of Hudson Bay. Characteristic shear of a low pressure system can be observed in Figure 4-20, demonstrating the correlation between the Southern Oscillation Index and zonal winds (Parkinson et al., 1999). Movement of this weather pattern to the south could rapidly reverse wind direction creating a sea ice see-saw shifting the ice pack east to west, north to south. This is consistent with the data presented in Figure 4-18 of separated zonal or meridional motion regimes of the Hudson Bay ice pack.

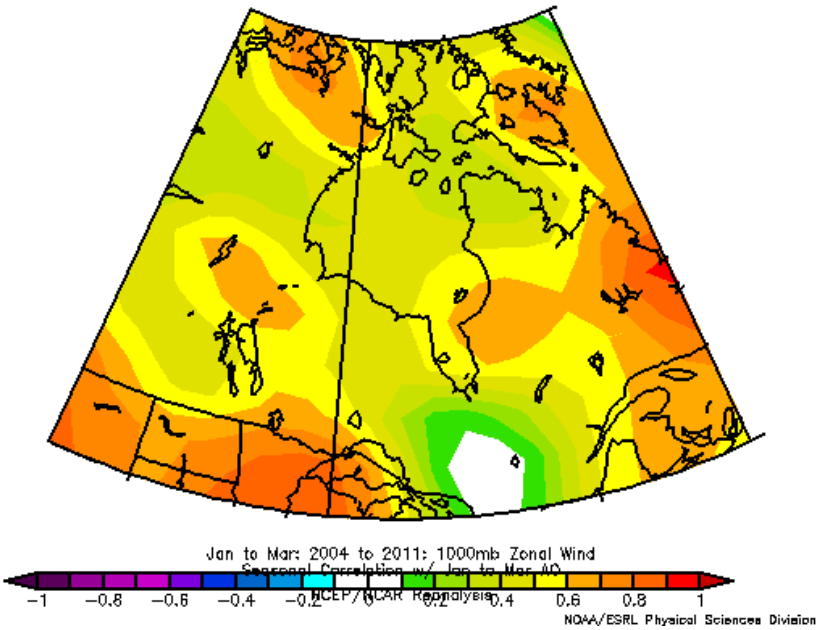

Figure 4-19 - JFM Correlation of NCEP Reanalysis Zonal Wind component and Arctic Oscillation Index 2004-2011.

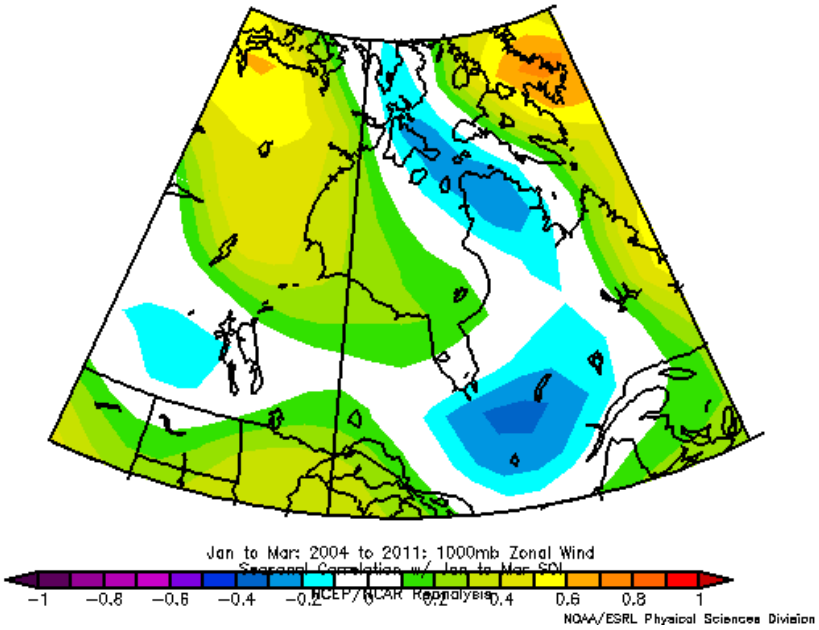

Figure 4-20 - JFM Correlation of NCEP Reanalysis Zonal Wind component and Southern Oscillation Index 2004-2011

4.2.3 *Freshwater Marine Coupling and Stratification*

If a semi-consolidated ice pack moves to reveal the open water surface, the ice displaced on the opposite coast must be deposited elsewhere. Where it goes depends on the properties of the pack ice and transfer of the flow (Wadhams, 2000). Prinsenberg (1988) suspected that significant ridging played major contributive roles to freshwater stratification across the bay. The existence and size of the northwest polynya suggests another influence on the redistribution of freshwater in Hudson Bay.

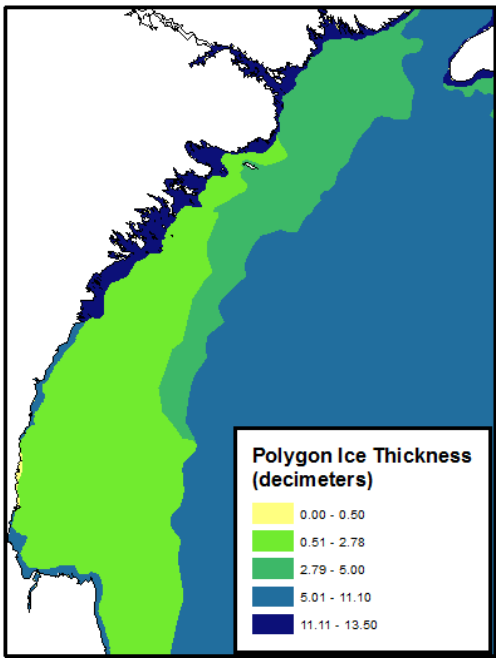

Figure 4-21 - Polygon ice thickness for CIS Hudson Bay Regional Ice Chart for March 29, 2010

Estimates from Canadian Ice Service operational ice charts demonstrate the northwest polynya area is characterized by thinner, more fractured ice than the rest of the bay. For example, following the significant polynya event described in §4.1.5, Figure 4-21 demonstrates replotted EGG code data as areal or polygon ice thickness (Equation 2; Ersahen et al., 2011). In an area slightly larger than the maximum observed polynya extent, there is a large expanse of ice thinner than 27.8 cm, while the central part of the bay exceeds 50 cm. This process was

observed in Figure 4-14 with frazil ice production accounting for the decline in open water extent; rather than the ice pack returning to its initial location from easterly wind forcing.

Thinner ice at the margin of a greater ice pack also has weaker strength, increasing susceptibility to ridging, rafting, and divergence. During frazil ice formation Langmuir rolls may be formed parallel to wind direction, further altering ice volume distribution in the polynya region. This is a pattern typical to late-season CIS charts data analyzed within the study period, adding support to the research hypothesis that the site of the northwestern polynya contributes significantly to ice production in the bay (Saucier et al., 2004). Significant ice production induces gravity mixing, and when it is localized over a small portion of the bay this may be a site of significant bottom water formation. Bay wide circulation reported in the literature as dominantly cyclonic would circulate this watermass at depth (Prinsenberg, 1986a).

The polynya may also condition water in regards to sea surface temperature (SST). Galbraith and Larouche (2011) found a positive relationship between earlier spring breakup dates, surface air temperature anomalies, and warmer maximum summer SST. Their subregion #18, along the northwest coast, demonstrated consistently low SST during the warmest week of each year. Conceptually the findings presented suggest that a longer period of incoming solar radiation may precondition the water, warming the low-albedo water mass faster than the surrounding icescape. The lack of high SST in the northwest suggests other factors, such as surface air temperature or upwelling of cooler water, may also affect stratification in this region.

Figure 4-22 demonstrates CTD data collected on ArcticNET Leg 1a in July 2010 along the MERICA transect (ArcticNet/Gratton 2010; Harvey et al., 2006). A much thinner western

summer mixed layer consistent with this conditioning hypothesis can be seen in the salinity data, while a temperature cross-section demonstrates more consistent temperature stratification across the bay. Ice production and resultant brine drainage and gravity mixing may contribute to the lower stratification in this region in addition to other causal factors (i.e. inbound Arctic water via Roes Welcome Sound, upwelling water masses, tidal mixing, winter conditioning due to brine rejection and gravity mixing, a thinner freshwater layer from melted sea ice, and northwestern river water input).

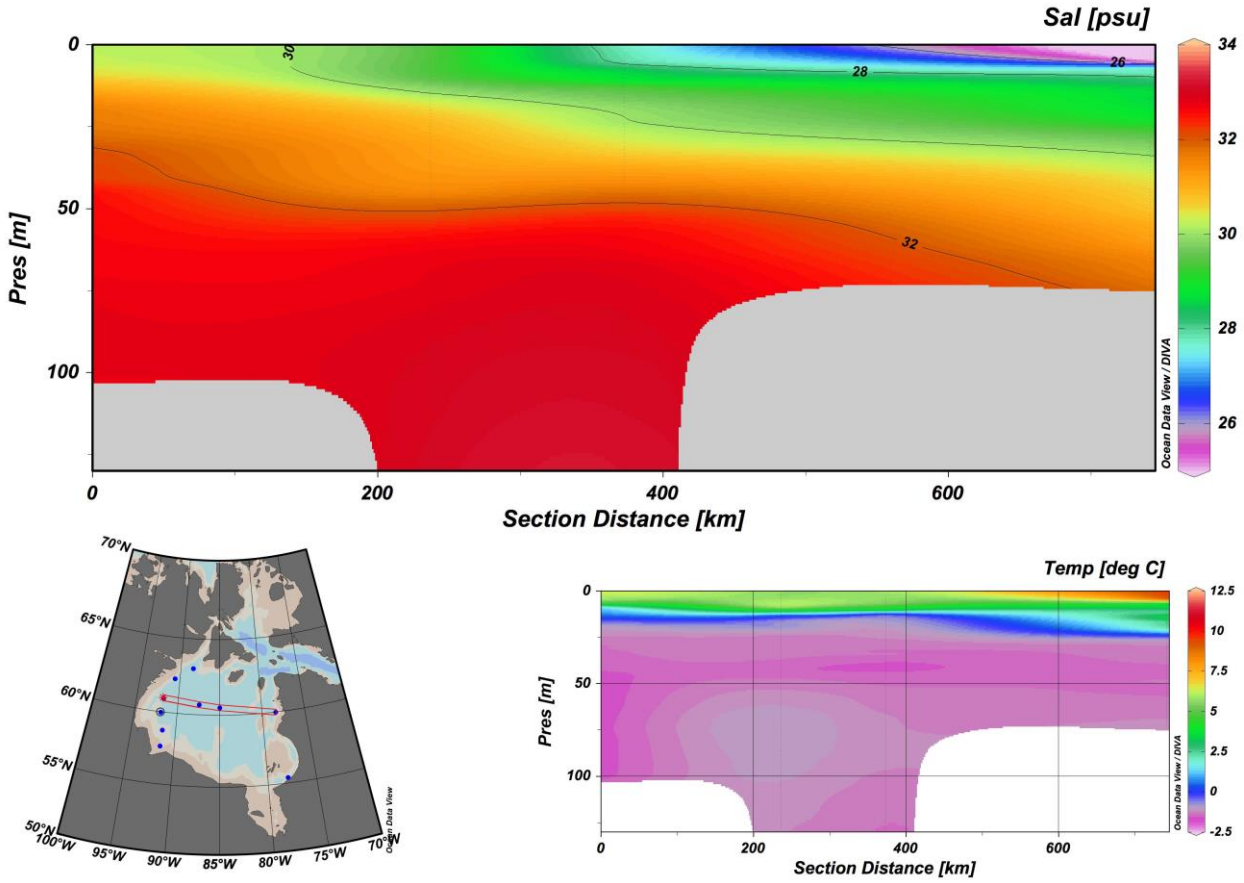

Figure 4-22 - Salinity/Temperature cross-section from ArcticNet 2010 Cruise 1a - July 2010 (ArcticNet/Gratton, 2010).

4.2.4 BIOLOGICAL IMPACTS

The polynya in northwestern Hudson Bay likely affects biota from autotrophs to pinnacle carnivores. The icescape of the region is an important habitat for the western Hudson Bay Polar Bears (*Ursus maritimus*); a solid barrier to air for overwintering marine mammals; and a growth medium for ice algae and pelagic phytoplankton.

A polynya in northwestern Hudson Bay may affect both light availability through recurrent openings and nutrient availability through increased mixing and reduced freshwater ice melt. Pelagic autotrophs experience a spring bloom once limitations on light, nutrients, or both are lifted (Sakshaug, 2004). Stratification is seen as a strong controlling mechanism on Hudson Bay primary production (Anderson and Roff, 1980; Ferland et al., 2011). Previous studies have demonstrated that Hudson Bay is an oligotrophic marine area, significantly limited by nutrients rather than sunlight. Persistent polynya openings with a high sun angle can alter the timing of bloom development, depleting biomass asynchronously to primary consumer growth phases (Maynard and Clark, 1987; Ji et al., 2013). Thinner ice cover, if in concert with reduced snow loading, can enhance the growth of ice algae which may go on to seed the spring bloom and lead to a rapid-but-brief event (Sakshaug and Skjoldal, 1989). While lower density stratification can enhance the nutrient load in the upper water, increased season length can deplete nutrients in the denser layer prior to temperature-induced stratification of the summer open water period (Arrigo et al., 1998; Carmack, 2007; Smetracek and Nicol, 2005).

Polynyas have demonstrated impacts on large marine fauna (e.g. Stirling, 1980; Dunbar, 1981; Stirling and Ramsay, 1986). Low biological diversity and few trophic linkages make larger fauna highly susceptible to environmental change, allowing changes to the environment to cascade through the ecosystem. Persistent open water on this western coast may be an

important key to understanding the western Polar Bear population, which requires open water leads and polynyas to hunt prey. Alterations to a sea ice regime can result in habitat loss for polar bears, ringed seals, and whales (Laidre et al., 2008; Tynan and DeMaster, 1997).

4.3 Suggested Further Research

Although this polynya and the greater coastal sea ice system in Hudson Bay has been known to researchers since the 1970s, there has been little specific research on the size, recurrence, and morphology of this important winter sea ice regime. The winter months and perennial ice cover are noted as a key factor to the physical and biological system of the Hudson Bay Marine Complex. This section discusses research priorities suggested by findings of this investigation.

Further research on polynya morphology, including stage of development of ice at high resolution may be undertaken with a series of fine synthetic aperture radar (SAR) images. This high resolution, cloud-penetrative data may provide greater spatial information about polynya size and the ice thickness gradient reaching into the central pack, and explore dynamic lead development processes. High resolution study of ice ridge morphology over the bay could further explain the origin and spatial distribution of the freshwater contribution of the ice melt layer.

Oceanography of the northwestern section of Hudson Bay could be studied in greater deal to find the relationship between inbound Arctic water through Roes Welcome Sound, existing bottom water, and the polar mixed layer. This could be done through the installation of moorings in this unique region, in addition to winter CTD and *in situ* physical ice investigations. Upward facing acoustic Doppler datasets on ice motion would be extremely

interesting for future research on this polynya. Continued physical investigation could confirm ice production models discussed in Saucier et al. (2004).

Atmospheric research is needed to determine the causal and maintenance factors of the Baffin Island low pressure system and how changing global climate conditions may affect it, and in turn the sea ice system of Hudson Bay. Continued research and observation is necessary for this system in its relationship to the stability and continental impacts of a weakened winter polar vortex. Changes to hemispheric climatic patterns could strongly influence recurrence and persistence of this polynya. Application of a one-dimensional model to this polynya would further examine contribution of dynamic versus thermodynamic constituents of forcing (van Woert, 1999).

There is a clear need for continued research into the spatial distribution of primary production in Hudson Bay. Current limitations in retrieval of surface chlorophyll-a due to river runoff, suspended sediments, and CDOM preclude high confidence in satellite measurement. Research into nutrient dynamics specific to the northwest portion of the bay could determine how mixing and Arctic waters are influencing primary production in this area. Moorings, discussed above, could also better track winter chlorophyll and nutrient loads as well as influences of stratification on the water mass. Limited *in situ* investigations show there is still much to be learned about this area.

Biological communities and trophic relationships should be studied with the frequency and opening period of this polynya in mind. The bi-modal distribution of cumulative seasonal open water and frequency of small polynya events could reveal an influence in population and

breeding success of large marine fauna and avian populations that depend on open water during the winter.

Transportation studies, especially between the populated places of western Hudson Bay, could reveal a winter resupply path between these with sufficiently ice-strengthened vessels. While a path to the global ocean does not appear to be practical during winter months at present, alterations in atmospheric forcing could change the ice regime enough to make winter marine transport a possibility.

5 CONCLUSION

This thesis demonstrated the existence and spatial-temporal characteristics of a polynya in northwestern Hudson Bay and explored the greater coastal polynya system during winter months. A large, recurring area of open water exists along the northwestern coastline from Churchill, MB to the mouth of Roes Welcome Sound extending from the fast ice margin to a variable distance offshore. This area displays the recurrent spatial character of a coastal polynya, rather than variable nature of a shore lead. The primary forcing mechanism of this polynya appears to be persistent westerly winds forced by either a frequent trough between cold Arctic air and cool midlatitude air, or a Baffin Island low pressure system. Maintenance of the polynya may be warmer winds from the southwest, however the balance between dynamic momentum transfer and thermodynamic heat loss can be very fine as demonstrated in the case study. This suggests considerable ice production localized to the study area, causing cascading effects to the greater marine system. Physical effects may include considerable brine rejection and associated lessened stratification, weakened ice strength, and increased solar radiation inputs. No change was noted over the eight season study period in size or frequency of this polynya during the winter.

As this is the first investigation to focus entirely on the polynya in northwestern Hudson Bay, it reveals there is still much to learn about the world's largest northern inland sea. Given the history of rapid change in the climate and sea ice regime of Hudson Bay, continuous observation is a requirement for reasonable management of this ecosystem. Considerable work at different spatial and temporal scales should

continue as this polynya and shore lead system may have significant impacts on the marine, atmospheric, and ecological systems of this central Canadian basin.

6 APPENDIX

6.1 WORKS CITED

Aagaard, K., and E. C. Carmack (1989), The role of fresh water in ocean circulation and climate, *J. Geophys. Res.*, *94*(Figure 1), 14485–14498.

Aagaard, K., and R. A. Woodgate (2001), Some Thoughts on the Freezing and Melting of Sea Ice and Their Effects on the Ocean, *Ocean Model.*, *3*, 127-135.

Aagaard, K., L. K. Coachman, and E. C. Carmack (1981), On the Halocline of the Arctic Ocean, *Deep Sea Res. Part I Oceanogr. Res. Pap.*, *28*(6), doi:10.1016/0198-0149(81)90115-1.

ACIA (2005). Cryosphere and Hydrology, in *Arctic Climate Impact Assessment*, Cambridge University Press, Cambridge, UK.

Ambaum, M. H., B. J. Hoskin, and D. B. Stephenson (2001), Arctic Oscillation or North Atlantic Oscillation?, *J. Clim.*, *14*(16), 3495–3508.

Anderson, J. T., and J. C. Roff (1980), Seston Ecology of the Surface Waters of Hudson Bay, *Can. J. Fish. Aquat. Sci.*, *37*, 2242–2253.

Arrigo, K. R., and G. L. van Dijken (2003), Phytoplankton dynamics within 37 Antarctic coastal polynya systems, *J. Geophys. Res.*, *108*(C8), 3271, doi:10.1029/2002JC001739.

Arrigo, K. R., A. M. Weiss, and W. O. Smith (1998), Physical forcing of phytoplankton dynamics, *J. Geophys. Res.*, *103*, 1007–1021.

Arrigo, K. R., D. H. Robinson, R. B. Dunbar, A. R. Leventer, and M. P. Lizotte (2003), Physical control of chlorophyll a , POC, and TPN distributions in the pack ice of the Ross Sea, Antarctica, *J. Geophys. Res.*, *108*(C10), 3316, doi:10.1029/2001JC001138.

Arrigo, K. R., K. E. Lowry, and G. L. van Dijken (2012), Annual changes in sea ice and phytoplankton in polynyas of the Amundsen Sea, Antarctica, *Deep Sea Res. Part II Top. Stud. Oceanogr.*, *71-76*, 5–15, doi:10.1016/j.dsr2.2012.03.006.

Assur, A., and W. F. Weeks (1964), Growth, Structure and Strength of Sea Ice. Cold Regions Research and Engineering Laboratory Monographs. Research Report No. 135. Hanover, NH. U.S. Army Materiel Command.

Babko, O., D. A. Rothrock, and G. A. Maykut (2002), Role of rafting in the mechanical redistribution of sea ice thickness, *J. Geophys Res.*, *107*(C8), doi:10.1029/1999JC000190.

Barber, D. G. (2005), Microwave Remote Sensing, Sea ice and Arctic Climate, *Phys. Canada*, *61*(5), 105–111.

Barber, D. G., and R. A. Massom (2007), The Role of Sea Ice in Arctic and Antarctic Polynyas, in *Polynyas: Windows to the World*, edited by W. O. Smith and D. G. Barber, pp. 1–54, Elsevier Science, Amsterdam.

Bareiss, J., and K. Görgen (2005), Spatial and temporal variability of sea ice in the Laptev Sea: Analyses and review of satellite passive-microwave data and model results, 1979 to 2002, *Glob. Planet. Change*, *48*(1-3), 28–54, doi:10.1016/j.gloplacha.2004.12.004.

Behrenfeld, M. J. (2010), Abandoning Sverdrup's Critical Depth Hypothesis on phytoplankton blooms., *Ecology*, *91*(4), 977–989.

Bhiry, N. et al. (2011), Environmental Change in the Great Whale River Region, Hudson Bay: Five Decades of Multidisciplinary Research by Centre d'études Nordiques (CEN), *Ecoscience*, *18*(3), 182–203, doi:10.2980/18-3-3469.

Bjørgo, E., O. M. Johannessen, and M. W. Miles (1997), Analysis of merged SMMR-SSMI time series of Arctic and Antarctic sea ice parameters 1978-1995, *Geophys. Res. Lett.*, *24*(4), 413–416.

Bromwich, D. H., and D. D. Kurtz (1984), Katabatic wind forcing of the Terra Nova Bay polynya, *J. Geophys. Res.*, *89*(4), 3561–3572, doi:10.1029/JC089iC03p03561.

Canadian Ice Service (2005), *Manual of Standard Procedures for Observing and Reporting Ice Conditions*, 9th edition, Environment Canada, Ottawa, ON.

Canadian Ice Service (2006), *Canadian Ice Service Digital Archive – Regional Charts: History, Accuracy, and Caveats*, Environment Canada, Ottawa, ON.

Cape, M. R., M. Vernet, M. Kahru, and G. Spreen (2014), Polynya dynamics drive primary production in the Larsen A and B embayments following ice shelf collapse, *J. Geophys. Res. Ocean.*, *119*(1), 572–594, doi:10.1002/2013JC009441.

Carmack, E. C. (2007), The alpha/beta ocean distinction: A perspective on freshwater fluxes, convection, nutrients and productivity in high-latitude seas, *Deep Sea Res. Part II Top. Stud. Oceanogr.*, *54*(23-26), 2578–2598, doi:10.1016/j.dsr2.2007.08.018.

Cavalieri, D. J., and S. Martin (1985), A passive microwave study of polynyas along the Antarctic Wilkes Land coast, in *Oceanology of the Antarctic Continental Shelf*, edited by S. S. Jacobs, pp. 227–252, American Geophysical Union, Washington D.C.

Cavalieri, D. J., and S. Martin (1994), The contribution of Alaskan, Siberian, and Canadian coastal polynyas to the cold halocline layer of the Arctic Ocean, *J. Geophys. Res.*, *99*(C9), 18343, doi:10.1029/94JC01169.

Cavalieri, D. J., B. A. Burns, and R. G. Onstott (1990), Investigation of the effects of summer melt on the calculation of sea ice concentration using active and passive microwave data, *J. Geophys. Res.*, *95*(C4), 5359, doi:10.1029/JC095iC04p05359.

Cavalieri, D. J., K. M. Stgermain, and C. T. Swift (1995), Reduction of weather effects in the calculation of sea ice concentration with the DMSP SSM/I, *J. Glaciol.*, *41*(139), 455–464.

Cavalieri, D. J., P. Gloersen, C. L. Parkinson, J. C. Comiso, and H. J. Zwally (1997), Observed Hemispheric Asymmetry in Global Sea Ice Changes, *Science.*, *278*, 1104–1106, doi:10.1126/science.278.5340.1104.

Cavalieri, D. J., C. L. Parkinson, P. Gloersen, J. C. Comiso, and H. J. Zwally (1999), Deriving long-term time series of sea ice cover from satellite passive-microwave multisensor data sets, *J. Geophys. Res.*, *104*(C7), 15803, doi:10.1029/1999JC900081.

Cerveny, R. S., B. M. Svoma, R. C. Balling, and R. S. Vose (2008), Gregorian calendar bias in monthly temperature databases, *Geophys. Res. Lett.*, *35*(19), L19706, doi:10.1029/2008GL035209.

Chambellant, M., I. Stirling, W. A. Gough, and S. H. Ferguson (2012), Temporal variations in Hudson Bay ringed seal (*Phoca hispida*) life-history parameters in relation to environment, *J. Mammal.*, *93*(1), 267–281, doi:10.1644/10-MAMM-A-253.1.

Comiso, J. C. (2010), *Polar Oceans from Space*, Springer, New York, NY.

Comiso, J. C., and H. J. Zwally (1989), *Polar microwave brightness temperatures from Nimbus-7 SMMR: Time series of daily and monthly maps from 1978 to 1987. NASA Reference Publn. RP1223*, Washington D.C.

Comiso, J. C., and R. Kwok (1996), Surface and radiative characteristics of the summer Arctic sea ice cover from multisensor satellite observations, *J. Geophys. Res.*, *101*(96), 28397–28416.

Cox, G. F. N., and W. F. Weeks (1975), *Brine drainage and initial salt entrapment in sodium chloride ice. CRREL Research Report 354*, United States Army Corps of Engineers, Hanover, NH.

Danielson, E. W. (1971), Hudson Bay Ice Conditions, *Arctic*, *24*(2), 90–107.

De Beurs, K. M., and G. M. Henebry (2005), A statistical framework for the analysis of long image time series, *Int. J. Remote Sens.*, *26*(8), 1551–1573, doi:10.1080/01431160512331326657.

Déry, S. J., M. Stieglitz, E. C. McKenna, and E. F. Wood (2005), Characteristics and Trends of River Discharge into Hudson , James , and Ungava Bays , 1964 – 2000, *J. Clim.*, *18*, 2540–2558.

Déry, S. J., T. J. Mlynowski, M. a. Hernández-Henríquez, and F. Straneo (2011), Interannual variability and interdecadal trends in Hudson Bay streamflow, *J. Mar. Syst.*, *88*(3), 341–351, doi:10.1016/j.jmarsys.2010.12.002.

Dey, B., H. Moore, and A. F. Gregory (1979), Monitoring and Mapping Sea-Ice Breakup and Freezeup of Arctic Canada from Satellite Imagery, *Arct. Alp. Res.*, *11*(2), 229–242.

Dieckmann, G. S., and H. H. Hellmer (2009), The Importance of Sea Ice: An Overview, in *Sea Ice*, edited by D. N. Thomas and G. S. Dieckmann, pp. 1–110, Wiley-Blackwell, Oxford.

Dragon, A.C., M.N. Houssais, C. Herbaut, and J.-B. Charrassin (2014), A note on the intraseasonal variability in an Antarctic polynia: Prior to and after the Mertz Glacier calving, *J. Mar. Syst.*, *130*, 46–55, doi:10.1016/j.jmarsys.2013.06.006.

Drinkwater, K. F., and E. P. Jones (1987), Density stratification, nutrient and chlorophyll distribution in the Hudson Strait region during summer and their relation to tidal mixing, *Cont. Shelf Res.*, *7*(6), 599–607, doi:10.1016/0278-4343(87)90025-2.

Dunbar, M. J. (1981), Physical Causes and biological significance of polynyas and other open water in sea ice, in *Polynyas in the Canadian Arctic*, edited by I. Stirling and H. Cleator, pp. 29–43, Canadian Wildlife Service, Ottawa, ON.

Dyck, M. G., W. Soon, R. K. Baydack, D. R. Legates, S. Baliunas, T. F. Ball, and L. O. Hancock (2007), Polar bears of western Hudson Bay and climate change: Are warming spring air temperatures the “ultimate” survival control factor?, *Ecol. Complex.*, *4*(3), 73–84, doi:10.1016/j.ecocom.2007.03.002.

Ersahin, K. M., M. Martínez de Saavedra Álvarez, D. Fissel, R. Kerr, and G. Borstad (2011), *Analysis of Polynya-Like Features in Foxe Basin*, Prepared for LGL Ltd. on behalf of BaffinLand Iron Mines Corp. ASL Environmental Services, Victoria, BC.

Etkin, D. A. (1991), Break-up in Hudson Bay : Its Sensitivity to Air Temperatures and Implications for Climate Warming, *Climatol. Bull.*, 21–34.

Ferland, J., M. Gosselin, and M. Starr (2011), Environmental control of summer primary production in the Hudson Bay system: The role of stratification, *J. Mar. Syst.*, *88*(3), 385–400, doi:10.1016/j.jmarsys.2011.03.015.

Fetterer, F., and N. Untersteiner (1998), Observations of melt ponds on Arctic sea ice, *J. Geophys. Res.*, *103*(Cll), 24821–24835.

Francis, J. A., and S. J. Vavrus (2012), Evidence linking Arctic amplification to extreme weather in mid-latitudes, *Geophys. Res. Lett.*, *39*(6), doi:10.1029/2012GL051000.

Freeman, N. G., and T. S. Murty (1976), Numerical modelling of tides in Hudson Bay, *J. Fish. Res. Board Canada*, *33*, 2345–2361.

Fu, H., J. Zhao, and K. E. Frey (2012), Investigation of polynya dynamics in the northern Bering Sea using greyscale morphology image-processing techniques, *Int. J. Remote Sens.*, *33*(7), 2214–2232, doi:10.1080/01431161.2011.608088.

Gagnon, A. S., and W. A. Gough (2005a), Climate change scenarios for the Hudson Bay Region: an intermodel comparison, *Clim. Change*, *69*, 269–297.

Gagnon, A. S., and W. A. Gough (2005b), Trends in the Dates of Ice Freeze-up and Breakup over Hudson Bay, Canada, *Arctic*, *58*(4), 370–382.

Galbraith, P. S., and P. Larouche (2011), Sea-surface temperature in Hudson Bay and Hudson Strait in relation to air temperature and ice cover breakup, 1985–2009, *J. Mar. Syst.*, *87*, 66–78, doi:10.1016/j.jmarsys.2011.03.002.

Galley, R. J., E. Key, D. G. Barber, B. J. Hwang, and J. K. Ehn (2008), Spatial and temporal variability of sea ice in the southern Beaufort Sea and Amundsen Gulf: 1980–2004, *J. Geophys. Res.*, *113*(C5), 1–18, doi:10.1029/2007JC004553.

Gough, W. A., and T. Allakhverdova (1998), Sensitivity of a coarse resolution ocean general circulation model under climate change forcing, *Tellus*, *50*(A), 124–133.

Gough, W. A., and E. Wolfe (2001), Climate Change Scenarios for Hudson Bay, Canada , from General Circulation Models, *Arctic*, *54*(2), 142–148.

Gough, W. A., A. S. Gagnon, and H. P. Lau (2004a), Interannual Variability of Hudson Bay Ice Thickness, *Polar Geogr.*, *28*(3), 222–238, doi:10.1080/789610188.

Gough, W. A., A. R. Cornwell, and L. J. S. Tsuji (2004b), Trends in Seasonal Sea Ice Duration in Southwestern Hudson Bay, *Arctic*, *57*(3), 299–305.

Granskog, M. A., R. W. Macdonald, Z. Z. a. Kuzyk, S. Senneville, C.-J. Mundy, D. G. Barber, G. a. Stern, and F. Saucier (2009), Coastal conduit in southwestern Hudson Bay (Canada) in summer: Rapid transit of freshwater and significant loss of colored dissolved organic matter, *J. Geophys. Res.*, *114*(C8), C08012, doi:10.1029/2009JC005270.

Grenfell et al.(1992), Considerations for microwave remote sensing of thin sea ice, in *Microwave Remote Sensing of Sea Ice*, edited by F. D. Carsey, American Geophysical Union, Washington D.C.

Gyakum, J. R., D. Zhang, J. Witte, K. Thomas, and W. Wintels (1996), CASPII and the Canadian cyclones during the 1989–92 cold seasons, *Atmosphere-Ocean*, *34*(1), 1–16, doi:10.1080/07055900.1996.9649555.

Hall, R. T., and D. A. Rothrock (1987), Photogrammetric observations of the lateral melt of sea ice floes, *J. Geophys. Res.*, *92*(C7), 7045, doi:10.1029/JC092iC07p07045.

Hare, F. K., and M. R. Montgomery (1949), Ice, open water, and winter climate in the eastern Arctic of North America, *Arctic*, *2*, 79–89.

Harvey, M., M. Starr, J. Therriault, F. J. Saucier, and M. Gosselin (2006), MERICA-Nord Program: Monitoring and Research in the Hudson Bay Complex, *AZMP Bull.*, *5*, 27–32.

Heinrichs, J. F., D. J. Cavalieri, and T. Markus (2006), Assessment of the AMSR-E Sea Ice-Concentration Product at the Ice Edge Using RADARSAT-1 and MODIS Imagery, *IEEE Trans. Geosci. Remote Sens.*, *44*(11), 3070–3080, doi:10.1109/TGRS.2006.880622.

Hinzman, L. D. et al. (2005), Evidence and Implications of Recent Climate Change in Northern Alaska and Other Arctic Regions, *Clim. Change*, *72*(3), 251–298, doi:10.1007/s10584-005-5352-2.

Hochheim, K. P., and D. G. Barber (2010), Atmospheric forcing of sea ice in Hudson Bay during the fall period, 1980–2005, *J. Geophys. Res.*, *115*(C5), 1–20, doi:10.1029/2009JC005334.

Hochheim, K., D. G. Barber, and J. V. Lukovich (2010), Changing Sea Ice Conditions in Hudson Bay, in *A Little Less Arctic: Top Predators in the World's Largest*

Northern Inland Sea, Hudson Bay, edited by S. H. Ferguson, L. L. Loseto, and M. L. Mallory, Springer Netherlands, Dordrecht.

Hochheim, K. P., J. V. Lukovich, and D. G. Barber (2011), Atmospheric forcing of sea ice in Hudson Bay during the spring period, 1980–2005, *J. Mar. Syst.*, *88*(3), 476–487, doi:10.1016/j.jmarsys.2011.05.003.

Holland, D. M., and L. A. Mysak (1996), Simulation of the mixed-layer circulation in the Arctic Ocean, *J. Geophys. Res. Ocean.*, *101*(95), 1111–1128, doi:10.1029/95JC02819.

Hwang, B. J. (2007), Retrieval of Geophysical and Thermodynamic state information from time series microwave radiometry in the fall and spring periods over Arctic sea ice, PhD thesis, 357 pp., University of Manitoba.

IHO (1971), *Limits of Oceans and Seas*, 3rd ed., International Hydrographic Organization Monte-Carlo, Monaco.

IPCC (2013), Observations: Cryosphere, in: *Climate Change 2013: The Physical Science Basis. Contribution of Working Group I to the Fifth Assessment Report of the Intergovernmental Panel on Climate Change* edited by T.F. Stocker, D. Qin, G.-K. Plattner, M. Tignor, S.K. Allen, J. Boschung, A. Nauels, Y. Xia, V. Bex and P.M. Midgley. Cambridge University Press, Cambridge UK and New York, NY.

Jacobs, S. S., and J. C. Comiso (1993), A recent sea ice retreat west of the Antarctic peninsula, *Geophys. Res. Lett.*, *20*(12), 1171–1174.

Jardon, F. P., F. Vivier, P. Bouruet-Aubertot, a. Lourenço, Y. Cuypers, and S. Willmes (2014), Ice production in Storfjorden (Svalbard) estimated from a model based on AMSR-E observations: Impact on water mass properties, *J. Geophys. Res. Ocean.*, *119*(1), 377–393, doi:10.1002/2013JC009322.

Ji, R., M. Jin, and Ø. Varpe (2013), Sea ice phenology and timing of primary production pulses in the Arctic Ocean., *Glob. Chang. Biol.*, *19*(3), 734–41, doi:10.1111/gcb.12074.

Joly, S., S. Senneville, D. Caya, and F. J. Saucier (2010), Sensitivity of Hudson Bay Sea ice and ocean climate to atmospheric temperature forcing, *Clim. Dyn.*, *36*(9-10), 1835–1849, doi:10.1007/s00382-009-0731-4.

Jones, E. P., and L. G. Anderson (1994), Northern Hudson Bay and Foxe Basin: Water masses, circulation and productivity, *Atmosphere-Ocean*, *32*(2), 361–374.

Kaleschke, L., C. Lupkes, T. Vihma, J. Haarpainter, A. Bochert, J. Hartmann, and G. Heygster (2001), SSM/I sea ice remote sensing for mesoscale ocean-

atmosphere interaction analysis: Ice and icebergs, *Can. J. Remote Sens.*, *27*(5), 526–537.

Kalnay, E. et al. (1996), The NCEP/NCAR 40-year reanalysis project, *Bull. Am. Meteorol. Soc.*, *77*(3), 437–471.

Kato, H., and O. M. Phillips (1969), On penetration of a turbulent layer into stratified fluid, *J. Fluid Mech.*, *37*, 643–655.

Kern, S. (2008), Polynya Area in the Kara Sea, Arctic, Obtained With Microwave Radiometry for 1979–2003, *IEEE Geosci. Remote Sens. Lett.*, *5*(2), 171–175, doi:10.1109/LGRS.2008.916831.

Kern, S. (2009), Wintertime Antarctic coastal polynya area: 1992–2008, *Geophys. Res. Lett.*, *36*(14), L14501, doi:10.1029/2009GL038062.

Kern, S., G. Spreen, L. Kaleschke, S. De La Rosa, and G. Heygster (2007), Polynya Signature Simulation Method polynya area in comparison to AMSR-E 89 GHz sea ice concentrations in the Ross Sea and off the Adelie Coast, Antarctica, for 2002-05: first results, *Ann. Glaciol.*, *46*(1), 1–10.

Kirillov, S. A., I. A. Dmitrenko, J. A. Hölemann, H. Kassens, and E. Bloshkina (2013), The penetrative mixing in the Laptev Sea coastal polynya pycnocline layer, *Cont. Shelf Res.*, *63*(March 2008), 34–42, doi:10.1016/j.csr.2013.04.040.

Kowalik, Z., and A. Y. Proshutinsky (1994), The Arctic Ocean tides, in *The Polar Oceans and Their Role in Shaping the Global Environment, Geophys. Monogr. Ser. vol 85*, edited by O. M. Johannessen, R. D. Muench, and J. E. Overland, pp. 137–158, American Geophysical Union, Washington D.C.

Kuzyk, Z. a., R. W. Macdonald, M. a. Granskog, R. K. Scharien, R. J. Galley, C. Michel, D. G. Barber, and G. Stern (2008), Sea ice, hydrological, and biological processes in the Churchill River estuary region, Hudson Bay, *Estuar. Coast. Shelf Sci.*, *77*(3), 369–384, doi:10.1016/j.ecss.2007.09.030.

Laidre, K. L., M. P. Heide-Jørgensen, J. Nyeland, A. Mosbech, and D. Boertmann (2008), Latitudinal gradients in sea ice and primary production determine Arctic seabird colony size in Greenland., *Proc. Biol. Sci.*, *275*(1652), 2695–702, doi:10.1098/rspb.2008.0874.

Lammers, R. B., A. I. Shiklomanov, C. J. Vörösmarty, B. M. Fekete, and B. J. Peterson (2001), Assessment of contemporary Arctic river runoff based on observational discharge records, *J. Geophys. Res.*, *106*(D4), 3321, doi:10.1029/2000JD900444.

Larouche, P., and J.-M. M. Dubois (1990), Dynamical evaluation of the surface circulation using remote sensing of drifting ice floes, *J. Geophys. Res.*, *95*(C6), 9755, doi:10.1029/JC095iC06p09755.

Lemke, P. (2001), Open the Windows to Polar Oceans, *Science*, 292(5522), 1670–1671.

Lillesand, T. M., R. W. Kiefer, and J. W. Chipman (2008), *Remote sensing and image interpretation*, 6th ed., Wiley, New York, NY.

Liu, A. K., S. Martin, and R. Kwok (1997), Tracking of Ice Edges and Ice Floes by Wavelet Analysis of SAR Images, *J. Atmos. Ocean. Technol.*, *14*, 1187–1199.

Lubin, D., and R. A. Massom (2004), *Polar Remote Sensing: Volume 1 Atmosphere and Oceans*, Praxis Publishing Ltd., Chichester, UK.

Lunn, N. J., I. Stirling, D. Andriashek, and G. B. Kolenosky (1997), Re-Estimating the Size of the Polar Bear Population in Western Hudson Bay, *Arctic*, *50*(3), 234–240.

Markham, W. E. (1986), The Ice Cover, in *Canadian Inland Seas*, edited by I. P. Martini, pp. 101–116, Elsevier, Amsterdam.

Markus, T., and B. A. Burns (1995), A method to estimate subpixel-scale coastal polynyas with satellite passive microwave data, *J. Geophys. Res.*, *100*(C3), 4473–4487.

Markus, T., J. C. Stroeve, and J. Miller (2009), Recent changes in Arctic sea ice melt onset, freezeup, and melt season length, *J. Geophys. Res.*, *114*(C12), C12024, doi:10.1029/2009JC005436.

Martin, S., and D. J. Cavalieri (1989), Contributions of the Siberian Shelf Polynyas to the Arctic Ocean Intermediate and Deep Water, *J. Geophys. Res.*, *94*(C9), 725–738.

Martini, I. P. (1986), The Coastal Features of Canadian Inland Seas, in *Canadian Inland Seas*, edited by I. P. Martini, pp. 117–142, Elsevier, Amsterdam.

Massom, R. A. (1988), The biological significance of open water within the sea ice covers of the polar regions, *Endeavour*, *12*(1), 21–27.

Massom, R. A., P. T. Harris, K. J. Michael, and M. J. Potter (1998), The distribution and formative processes of latent-heat polynyas in East Antarctica, *Ann. Glaciol.*, *27*, 420–426.

Massom, R. A., S. E. Stammerjohn, W. Lefebvre, S. A. Harangozo, N. Adams, T. A. Scambos, M. J. Pook, and C. Fowler (2008), West Antarctic Peninsula sea ice in 2005: Extreme ice compaction and ice edge retreat due to strong anomaly with respect to climate, *J. Geophys. Res.*, *113*(C2), C02S20, doi:10.1029/2007JC004239.

Maxwell, J. B. (1986), A Climate Overview of Canadian Inland Seas, in *Canadian Inland Seas*, edited by I. P. Martini, pp. 79–99, Elsevier Science, Amsterdam.

Maykut, G. A. (1978), Energy exchange over young sea ice in the Central Arctic, *J. Geophys. Res.*, *83*(8), 3646–3658, doi:10.1029/JC083iC07p03646.

Maykut, G. A. (1982), Large-scale heat exchange and ice production in the Central Arctic, *J. Geophys. Res.*, *87*(C10), 7971–7984, doi:10.1029/JC087iC10p07971.

Maynard, N. G., and D. K. Clark (1987), Satellite color observations of spring blooming in Bering Sea shelf waters during ice edge retreat in 1980, *J. Geophys. Res.*, *92*, 7127–7139.

McGovern, P. G. (2013), East-West Asymmetry in Coastal Temperatures of Hudson Bay as a Proxy for Sea Ice, MSc. Thesis, 106 pp., University of Toronto.

Mcnutt, L. (1981), *Ice conditions in the eastern Bering Sea from NOAA and Landsat Imagery: Winter Conditions 1974, 1976, 1977, 1979, NOAA Tech. Memo. ERL PMEL-24*, 179 pp. Seattle, WA.

Melling, H., and E. L. Lewis (1982), Shelf drainage flows in the Beaufort Sea and their effect on the Arctic Ocean pycnocline, *Deep Sea Res.*, *29*, 967–985.

Mesinger, F. et al. (2006), North American Regional Reanalysis, *Bull. Am. Meteorol. Soc.*, *87*(3), 343–360, doi:10.1175/BAMS-87-3-343.

Morales Maqueda, M. A., A. J. Willmott, and N. R. T. Biggs (2004), Polynya Dynamics: A Review of Observations and Modeling, *Rev. Geophys.*, *42*(RG1004), doi:10.1029/2002RG000116.

Moroni, M., and A. Cenedese (2006), Nonlinear Processes in Geophysics Penetrative convection in stratified fluids : velocity and temperature measurements, *Nonlinear Process. Geophys.*, *13*(3), 353–363.

Mysak, L. A., R. G. Ingram, J. Wang, and A. van der Baaren (1996), The anomalous sea-ice extent in Hudson bay, Baffin bay and the Labrador sea during three simultaneous NAO and ENSO episodes, *Atmosphere-Ocean*, *34*(2), 313–343, doi:10.1080/07055900.1996.9649567.

NSIDC, All About Sea Ice: Data: Terminology, Available from: http://nsidc.org/cryosphere/seaice/data/terminology.html (Accessed 30 June 2014)

Oliver, J. E., and R. W. Fairbridge (Eds.) (1987), *The Encyclopedia of Climatology*, Nostrand Reinhold, New York.

Overland, J. E. (2014), Long-range linkage, *Nat. Clim. Chang.*, *4*, 11–12.

Parkinson, C. L. (2000), Variability of Arctic Sea Ice : The View from Space , An 18-Year Record, *Arctic*, *53*(4), 341–358.

Parkinson, C. L., D. J. Cavalieri, P. Gloersen, H. J. Zwally, and J. C. Comiso (1999), Arctic sea ice extents, areas, and trends, 1978-1996, *J. Geophys. Res.*, *104*(C9), 20837–20856.

Pease, C. H. (1987), The Size of Wind-Driven Coastal Polynyas, *J. Geophys. Res.*, *92*(7), 7049–7059.

Petrich, C., and H. Eicken (2010), Growth, structure and properties of sea ice, in *Sea Ice*, edited by D. N. Thomas and G. S. Dieckmann, pp. 23–77, Wiley-Blackwell, Hoboken, NJ.

Perovich, D. K. (2005), On the aggregate-scale partitioning of solar radiation in Arctic sea ice during the Surface Heat Budget of the Arctic Ocean (SHEBA) field experiment, *J. Geophys. Res.*, *110*(C3), 1–12, doi:10.1029/2004JC002512.

Pinto, J. O., J. a. Curry, and K. L. McInnes (1995), Atmospheric convective plumes emanating from leads: 1. Thermodynamic structure, *J. Geophys. Res.*, *100*(C3), 4621, doi:10.1029/94JC02654.

Pinto, J. O. (2003), Surface characteristics and atmospheric footprint of springtime Arctic leads at SHEBA, *J. Geophys. Res.*, *108*(C4), 8051, doi:10.1029/2000JC000473.

Piwowar, J. M. (2008), The derivation of an Arctic sea ice normal through temporal mixture analysis of satellite imagery, *Int. J. Appl. Earth Obs. Geoinf.*, *10*(1), 92–108, doi:10.1016/j.jag.2007.10.001.

Piwowar, J. M., and E. F. LeDrew (1995), Hypertemporal analysis of remotely sensed sea-ice data for climate change studies, *Prog. Phys. Geogr.*, *19*(2), 216–242, doi:10.1177/030913339501900204.

Piwowar, J. M., D. R. Peddle, and E. F. Ledrew (1998), Temporal Mixture Analysis of Arctic Sea Ice Imagery : A New Approach for Monitoring Environmental Change, *Remote Sens. Environ.*, *4257*(97), 195–207.

Prinsenberg, S. J. (1983), Effects of the hydroelectric developments on the oceanographic surface parameters of Hudson Bay, *Atmosphere-Ocean*, *21*(4), 418–430, doi:10.1080/07055900.1983.9649177.

Prinsenberg, S. J. (1984), Freshwater contents and heat budgets of James Bay and Hudson Bay, *Cont. Shelf Res.*, *3*(2), 191–200.

Prinsenberg, S. J. (1986a), The Circulation Pattern and Current Structure of Hudson Bay, in *Canadian Inland Seas*, edited by I. P. Martini, pp. 187–204, Elsevier, Amsterdam.

Prinsenberg, S. J. (1986b), Salinity and Temperature Distributions of Hudson Bay and James Bay, in *Canadian Inland Seas*, edited by I. P. Martini, pp. 163–186, Elsevier, Amsterdam.

Prinsenberg, S. J. (1988), Ice-Cover and Ice-Ridge Contributions to the Freshwater Contents, *Arctic*, *41*(1), 6–11.

Prinsenberg, S. J., and N. G. Freeman (1986), Tidal Heights and Currents in Hudson Bay and James Bay, in *Canadian Inland Seas*, edited by I. P. Martini, pp. 205–216, Elsevier, Amsterdam.

Prinsenberg, S. J., R. H. Loucks, R. E. Smith, and R. W. Trites (1987), Hudson Bay and Ungava Bay runoff cycles for the period 1963 to 1983. *Canad. Tech. Rep. Hydrog. Ocean. Sci. 92*(viii), 71.

Qian, M., C. Jones, R. Laprise, and D. Caya (2008), The Influences of NAO and the Hudson Bay sea-ice on the climate of eastern Canada, *Clim. Dyn.*, *31*(2-3), 169–182, doi:10.1007/s00382-007-0343-9.

Reddy, T. E., K. R. Arrigo, and D. M. Holland (2007), The role of thermal and mechanical processes in the formation of the Ross Sea summer polynya, *J. Geophys. Res.*, *112*(C7), C07027, doi:10.1029/2006JC003874.

Reed, R. J. (1960), Principal frontal zones of the Northern Hemisphere in winter and summer, *Bull. Am. Meteorol. Soc.*, *41*, 591–598.

Regehr, E. V., N. J. Lunn, S. C. Amstrup, and I. Stirling (2007), Effects of Earlier Sea Ice Breakup on Survival and Population Size of Polar Bears in Western Hudson Bay, *J. Wildl. Manage.*, *71*(8), 2673–2683, doi:10.2193/2006-180.

Röhrs, J., and L. Kaleschke (2012), An algorithm to detect sea ice leads by using AMSR-E passive microwave imagery, *Cryosph.*, *6*(2), 343–352, doi:10.5194/tc-6-343-2012.

Sakshaug, E. (2004), Primary and secondary production in the Arctic Seas, in *The Organic Carbon Cycle in the Arctic Ocean*, edited by R. Stein and R. W. Macdonald, pp. 57–81, Springer, New York, NY.

Sakshaug, E., and H. R. Skjoldal (2011), Life at the Ice Edge, *Ambio*, *18*(1), 60–67.

Saucier, F. J., S. Senneville, S. Prinsenberg, F. Roy, G. Smith, P. Gachon, D. Caya, and R. Laprise (2004), Modelling the sea ice-ocean seasonal cycle in Hudson Bay, Foxe Basin and Hudson Strait, Canada, *Clim. Dyn.*, *23*(3-4), 303–326, doi:10.1007/s00382-004-0445-6.

Schledermann, P. (1980), Polynyas and Prehistoric Settlement Patterns, *Arctic*, *33*(2), 292–302.

Scott, J. B. T., and G. J. Marshall (2010), A Step-Change in the Date of Sea-Ice Breakup in Western Hudson Bay, *Arctic*, *63*(2), 155–164.

Shiklomanov, I. A., A. I. Shiklomanov, R. B. Lammers, B. J. Peterson, and C. J. Vorosmarty (2000), The dynamics of river water inflow to the Arctic Ocean, in *The Freshwater Budget of the Arctic Ocean*, edited by E. L. Lewis, E. P. Jones, P. Lemke, T. D. Prowse, and P. Wadhams, pp. 281–296, Springer Netherlands, Dordrecht.

Sihvola, A. H., and J. A. Kong (1988), Effective permittivity of dielectric mixtures, *IEEE Trans. Geosci. Remote Sens.*, *26*(4), 420–429, doi:10.1109/36.3045.

Smetacek, V., and S. Nicol (2005), Polar ocean ecosystems in a changing world., *Nature*, *437*(7057), 362–8, doi:10.1038/nature04161.

Smith, M., and B. Rigby (1981), Distribution of polynyas in the Canadian Arctic, in *Polynyas in the Canadian Arctic*, edited by I. Stirling and H. Cleator, pp. 7–28, Canadian Wildlife Service, Ottawa, ON.

Smith, S. D., R. D. Muench, and C. H. Pease (1990), Polynyas and Leads: An Overview of Physical Processes and Environment, *J. Geophys. Res.*, *95*(April 1964), 9461–9479.

Smith, M. B., J.-P. Labat, A. D. Fraser, R. a. Massom, and P. Koubbi (2011), A GIS approach to estimating interannual variability of sea ice concentration in the Dumont d'Urville Sea near Terre Adélie from 2003 to 2009, *Polar Sci.*, *5*(2), 104–117, doi:10.1016/j.polar.2011.04.007.

Spreen, G., L. Kaleschke, and G. Heygster (2008), Sea ice remote sensing using AMSR-E 89-GHz channels, *J. Geophys. Res.*, *113*(C2), C02S03, doi:10.1029/2005JC003384.

Stewart, D. B., and D. G. Barber (2010), The Ocean-Sea Ice-Atmosphere System of the Hudson Bay Complex, in *A Little Less Arctic: Top Predators in the World's Lagest Northern Inland Sea, Hudson Bay*, edited by S. H. Ferguson, L. L. Loseto, and M. L. Mallory, Springer Netherlands, Dordrecht.

Stewart, D. B., and W. L. Lockhart (2005), Summary of the Hudson Bay Marine Ecosystem, *Can. Tech. Rep. Fish. Aquat. Sci.*, *2586*, 487.

Stewart, E. J., A. Tivy, S. E. L. Howell, J. Dawson, and D. Draper (2012), Cruise Tourism and Sea Ice in Canada's Hudson Bay Region, *Arctic*, *63*(1), 57–66.

Stirling, I. (1980), The Biological Importance of Polynyas in the Canadian Arctic, *Arctic*, *33*(2), 303–315.

Stirling, I., H. Cleator, and T.G. Smith (1981). Marine mammals, in *Polynyas in the Canadian Arctic*, edited by I. Stirling and H. Cleator. Canadian Wildlife Service Ocassional Paper 45. Ottawa, ON.

Stirling, I., and M. A. Ramsay (1986), Polar Bears in Hudson Bay and Foxe Basin: Present Knowledge and Research Opportunities, in *Canadian Inland Seas*, edited by I. P. Martini, pp. 341–354, Elsevier Science, Amsterdam.

Stirling, I., C. Jonkel, P. Smith, R. Roberson, and D. Cross (1977), *The ecology of the polar bear (Ursus maritimus) along the western coast of Hudson Bay. Canadian Wildlife Service Occasional Paper 33*, Canadian Wildlife Service, Ottawa, ON.

Stirling, I., N. J. Lunn, and J. Iacozza (1999), Hudson Bay in the Population Trends Ecology of Polar Bears in Western Hudson Bay in Relation to Climatic Change, *Arctic*, *52*(3), 294–306.

St-Laurent, P., F. Straneo, J.-F. Dumais, and D. G. Barber (2011), What is the fate of the river waters of Hudson Bay?, *J. Mar. Syst.*, *88*(3), 352–361, doi:10.1016/j.jmarsys.2011.02.004.

Straneo, F., and F. Saucier (2008), The outflow from Hudson Strait and its contribution to the Labrador Current, *Deep Sea Res. Part I Oceanogr. Res. Pap.*, *55*(8), 926–946, doi:10.1016/j.dsr.2008.03.012.

Stringer, W. J., and J. E. Groves (1991), Location and Areal Extent of Polynyas in the Bering and Chukchi Seas, *Arctic*, *4*(Supp.1), 164–171.

Stroeve, J. C., Serreze, M. C., Fetterer, F., Arbetter, T., Meier, W., Maslanik, J., and Knowles, K. (2005). Tracking the Arctic's shrinking ice cover: Another extreme September minimum in 2004. Geophysical Research Letters, 32(4), L04501. doi:10.1029/2004GL021810

Stroeve, J., M. C. Serreze, S. Drobot, S. Gearherd, M. Holland, J. Maslanik, T. Meier, and T. A. Scambos (2008), Arctic sea ice extent plummets in 2007, *EOS, Trans. Am. Geophys. Union*, *89*, 13–14. doi:10.1029/2008EO020001

Sverdrup, H. U. (1953), On conditions for the vernal blooming of phytoplankton, *J. du Cons. Int. pour l'Exploration la Mer*, 287–295.

Swift, C. T., D. J. Cavalieri, P. Gloersen, H. . J. Zwally, N. M. Mognard, W. J. Campbell, L. S. Fedor, and S. Peteherych (1985), Observations of the polar-regions from satellites using active and passive microwave techniques, *Adv. Geophys.*, *27*.

Tang, Q., X. Zhang, X. Yang, and J. a Francis (2013), Cold winter extremes in northern continents linked to Arctic sea ice loss, *Environ. Res. Lett.*, *8*(1), 014036, doi:10.1088/1748-9326/8/1/014036.

Thompson, D. W. J., and J. M. Wallace (1998), The Arctic Oscillation signature in the wintertime geopotential height and temperature, *Geophys. Res. Lett.*, *25*(9), 1297–1300.

Thordike (1975), The thickness distribution of sea ice, *J. Geophys. Res.*, *80*(33), 4501–4513, doi:10.1029/JC080i033p04501.

Thorndike, A. S., and R. Colony (1982), Sea ice motion in response to geostrophic winds, *J. Geophys. Res.*, *87*(C8), 5845–5852.

Tivy, A., B. Alt, S. Howell, K. Wilson, and J. Yackel (2007), Long-Range Prediction of the Shipping Season in Hudson Bay: A Statistical Approach, *Weather Forecast.*, *22*(5), 1063–1075, doi:10.1175/WAF1038.1.

Tivy, A., S. E. L. Howell, B. Alt, S. McCourt, R. Chagnon, G. Crocker, T. Carrieres, and J. J. Yackel (2011), Trends and variability in summer sea ice cover in the Canadian Arctic based on the Canadian Ice Service Digital Archive, 1960–2008 and 1968–2008, *J. Geophys. Res.*, *116*(C3), C03007, doi:10.1029/2009JC005855.

Troupin, C. et al. (2012), Generation of analysis and consistent error fields using the Data Interpolating Variational Analysis (DIVA), *Ocean Model.*, *52-53*, 90–101, doi:10.1016/j.ocemod.2012.05.002.

Tucker, W., D. K. Perovich, A. J. Gow, W. F. Weeks, and M. R. Drinkwater (1992), Physical properties of sea ice relevant to remote sensing, in *Microwave Remote Sensing of Sea Ice*, pp. 9–27, American Geophysical Union, Washington, D.C.

Tynan, C. T., and D. P. Demaster (1997), Observations and Predictions of Arctic Climatic Change : Potential Effects on Marine Mammals, *Arctic*, *50*(4), 308–322.

Untersteiner, N. (1968), Natural Desalination and Equilibrium Salinity Profile, *J. Geophys. Res.*, *73*(4), 1251–1257.

USHO (1946), *Sailing directions for northern Canada including the coast of Labrador north of St. Lewis Sound, the northern coast of the Canadian mainland, and the Canadian Archipelago*, United States Hydrographic Office, Washington D.C.

Van Woert, M. L. (1999), Wintertime dynamics of the Terra Nova Bay polynya, *J. Geophys. Res.*, *104*(C4), 7753–7769, doi:10.1029/1999JC900003.

Wadhams, P. (2000), *Ice in the ocean*, Taylor & Francis, New York, NY.

Wang, J., L. A. Mysak, and R. G. Ingram (1994), Interannual Variability of Sea-Ice Cover in Hudson Bay, Baffin Bay and the Labrador Sea, *Atmosphere-Ocean*, *32*(2), 421–447.

Weeks, W. F., and S. F. Ackley (1986), The growth, structure, and properties of sea ice, in *The Geophysics of Sea Ice: NATO ASI Series B: Physics vol. 146*, edited by N. Untersteiner, Plenum Press, New York, NY.

Wessel, P., and W. H. F. Smith (1996), A global, self-consistent, hierarchical, high-resolution shoreline, *J. Geophys. Res.*, *101*(96), 8741–8743.

Williams, W. J., E. C. Carmack, and R. G. Ingram (2007), Physical oceanography of polynyas, in *Polynyas: Windows to the World*, edited by W. O. Smith and D. G. Barber, pp. 55–85, Elsevier Science, Amsterdam.

Willmes, S., S. Adams, D. Schröder, and G. Heinemann (2011), Spatio-temporal variability of polynya dynamics and ice production in the Laptev Sea between the winters of 1979/80 and 2007/08, *Polar Res.*, *30*, 1–16, doi:10.3402/polar.v30i0.5971.

Winebrenner, D., et al. (1992), Microwave sea ice signature modeling, in *Microwave Remote Sensing of Sea Ice*, edited by F. D. Carsey, American Geophysical Union, Washington D.C.

Worby, A. P., and J. C. Comiso (2004), Studies of the Antarctic sea ice edge and ice extent from satellite and ship observations, *Remote Sens. Environ.*, *92*(1), 98–111, doi:10.1016/j.rse.2004.05.007.

6.2 Citations for Data Sources

Passive Microwave

ARTIST Sea Ice (ASI) AMSR-E sea ice concentration data obtained for 2003-2011 from the Integrated Climate Data Centre (ICDC, http://icdc.zmaw.de/), University of Hamburg, Hamburg, Germany.

For further information see Kaleschke et al. (2001) and Spreen et al. (2008)

Optical

NASA MODIS Composite Subsets from https://earthdata.nasa.gov/data/near-real-time-data/
The author acknowledges the use of Rapid Response imagery from the Land Atmosphere Near-real time Capability for EOS (LANCE) system operated by the NASA/GSFC/Earth Science Data and Information System (ESDIS) with funding provided by NASA/HQ.

USGS Landsat Thematic Mapper data acquired from United States Geological Survey Earth Explorer.

Coastlines

Global Self-consistent, Hierarchical, High-resolution Geography (GSHHG) intermediate resolution coastline data available at http://www.ngdc.noaa.gov/mgg/shorelines/gshhs.html .

For further information see Wessel and Smith (1996).

Gridded Climate Reanalyses

NCEP Reanalysis provided by NOAA/OAR/ESRL PSD, Boulder, Colorado, USA from their website at http://www.esrl.noaa.gov/psd

For further information see Kalnay et al. (1996)

The North American Regional Reanalysis (NARR) is a long-term, consistent, high-resolution climate dataset for the North American domain, as a major improvement upon early global reanalysis datasets in both resolution and accuracy.

For further information see Mesinger et al. (2006)

Surface Air Temperature

Air Temperature Data provided by the Environment Canada Digital Climate Archive (http://climate.weather.gc.ca)

Digitized Regional Ice Charts

Operational Ice Charts provided by the Canadian Ice Service in ESRI exchange (e00) format (http://www.ec.gc.ca/glaces-ice/)

In Situ *Oceanographic Data*

CTD Rosette data collected on ArcticNet 2010 Leg 1a aboard the CCGS *Amundsen*. Rosette operators Camil Hamel and Dominique Boisvert on behalf of Dr. Yves Gratton. Quality control and processing by Pascal Guillot and Yves Gratton.

6.3 Projection Details

Processing Projection Details
HudsonBay_Albers_Equal_Area_Conic
Authority: Custom
Projection: Albers
false_easting: 0.0
false_northing: 0.0
central_meridian: -38.0
standard_parallel_1: 58.0
standard_parallel_2: 62.0
latitude_of_origin: 50.0
Linear Unit: Meter (1.0)
Geographic Coordinate System: GCS_North_American_1983
Angular Unit: Degree (0.0174532925199433)
Prime Meridian: Greenwich (0.0)
Datum: D_North_American_1983
Spheroid: GRS_1980
Semimajor Axis: 6378137.0
Semiminor Axis: 6356752.314140356
Inverse Flattening: 298.257222101

6.4 Adjusted Date of Year Key

Season	aDOY 1 =	aDOY 90 =	aDOY 180 =	aDOY 270 =
2003/2004	September 2, 2003	November 30, 2003	February 28, 2004	May 28, 2004
2004/2005	September 1, 2004	November 29, 2004	February 27, 2005	May 28, 2005
2005/2006	September 1, 2005	November 29, 2005	February 27, 2006	May 28, 2006
2006/2007	September 2, 2006	November 30, 2006	February 28, 2007	May 29, 2007
2007/2008	September 2, 2007	November 30, 2007	February 28, 2008	May 28, 2008
2008/2009	September 1, 2008	November 29, 2008	February 27, 2009	May 28, 2009
2009/2010	September 1, 2009	November 29, 2009	February 27, 2010	May 28, 2010
2010/2011	September 1, 2010	November 29, 2010	February 27, 2011	May 28, 2011

6.5 Eigenvalues for Principal Components Analysis

Performed in ArcGIS 10.2 Spatial Analyst. Correlation-type analysis.

Component	% of Eigenvalues	Cumulative percent of Eigenvalues
1	46.372	46.372
2	21.177	67.546
3	8.215	75.763
4	6.66	82.419
5 – 12	17.581	100.000